

1
2
3 **A novel triptolide analog downregulates NF-κB and induces**
4 **mitochondrial apoptosis pathways in human pancreatic cancer**
5

6 Qiaomu Tian^{1#}, Peng Zhang^{2#}, Yihan Wang¹, Youhui Si¹, Dengping Yin¹, Christopher R Weber³,
7 Melissa L Fishel⁴, Karen E Pollok⁴, Bo Qiu², Fei Xiao², Anita S Chong^{1*}
8
9

10 ¹Department of Surgery, The University of Chicago, Chicago, IL

11 ²Cinkate Pharmaceutical Corp, ZhangJiang District, Shanghai

12 ³Department of Pathology, The University of Chicago, Chicago, IL

13 ⁴Department of Pediatrics, Indiana University, Indianapolis, IN
14
15
16
17
18
19

20 #These authors contributed equally
21

22 *To whom correspondence should be addressed:

23 Anita S. Chong, PhD

24 Professor, Section of Transplantation

25 Department of Surgery

26 The University of Chicago

27 5841 S. Maryland Ave

28 Chicago, IL60637

29 Email: achong@uchicago.edu

30 Tel: (773) 702-5521
31

Abstract

Pancreatic cancer is the seventh leading cause of cancer-related death worldwide, and despite advancements in disease management, the 5-year survival rate stands at only 12%. Triptolides have potent anti-tumor activity against different types of cancers, including pancreatic cancer, however poor solubility and toxicity limit their translation into clinical use. We synthesized a novel pro-drug of triptolide, (*E*)-19-[(1'-benzoyloxy-1'-phenyl)-methylidene]-Triptolide (CK21), which was formulated into an emulsion for *in vitro* and *in vivo* testing in rats and mice, and using human pancreatic cancer cell lines and patient-derived pancreatic tumor organoids. A time-course transcriptomic profiling of tumor organoids treated with CK21 *in vitro* was conducted to define its mechanism of action, as well as transcriptomic profiling at a single time point post-CK21 administration *in vivo*. Intravenous administration of emulsified CK21 resulted in the stable release of triptolide, and potent anti-proliferative effects on human pancreatic cancer cell lines and patient-derived pancreatic tumor organoids *in vitro*, and with minimal toxicity *in vivo*. Time course transcriptomic profiling of tumor organoids treated with CK21 *in vitro* revealed <10 differentially expressed genes (DEGs) at 3 h and ~8,000 DEGs at 12 h. Overall inhibition of general RNA transcription was observed, and Ingenuity pathway analysis together with functional cellular assays confirmed inhibition of the NF- κ B pathway, increased oxidative phosphorylation and mitochondrial dysfunction, leading ultimately to increased reactive oxygen species (ROS) production, reduced B-cell-lymphoma protein 2 (BCL2) expression, and mitochondrial-mediated tumor cell apoptosis. CK21 is a novel pro-drug of triptolide that exerts potent anti-proliferative effects on human pancreatic tumors by inhibiting the NF- κ B pathway, leading ultimately to mitochondrial-mediated tumor cell apoptosis.

Key Words: Triptolide, pancreatic cancer, apoptosis

55 Introduction

56
57 Pancreatic cancer is the seventh leading cause of cancer related deaths globally and the third
58 leading in the United States, and has the lowest 5-year survival rate among all the cancers¹.
59 Pancreatic ductal adenocarcinoma accounts for >90% of all pancreatic cancer cases, and poor
60 outcomes have been attributed to late diagnoses when the cancer is at advance stages², where the
61 majority of cases are accompanied with distant metastasis^{3,4} and when most patients are not eligible
62 for resection⁵. Fluorouracil, and gemcitabine are FDA approved as adjuvant chemotherapy after
63 pancreatic cancer resection⁶, FOLFIRINOX, Abraxane with gemcitabine represent first-line
64 chemotherapy for patients with metastatic pancreatic cancer⁷⁻⁹. For patients with resectable disease
65 followed by adjuvant chemotherapy, anticipated median overall survival is 54.4 months, however, for
66 patients with advanced unresectable disease, the survival benefit with multiagent chemotherapy is
67 only 2-6 months².

68 The Chinese herb, *Tripterygium wilfordii* hook F (Thunder God vine), has anti-inflammatory,
69 immunosuppressive, contraceptive, and anti-tumor activities, and has been used for centuries as
70 traditional Chinese medicine for treating rheumatoid arthritis and lupus. In 1972, Morris *et al.*
71 extracted triptolide from *T. wilfordii* and characterized it as a structurally unique diterpene triepoxide,
72 with potential anti-leukemic properties¹⁰. Subsequently, triptolide was shown to have anti-tumor
73 effects in pre-clinical mouse models of breast cancer^{11,12}, cholangiocarcinoma¹³, osteosarcoma¹⁴,
74 lung cancer^{15,16}, acute myeloid leukemia^{17,18}, ovarian cancer^{19,20}, prostate cancer²¹, gastric cancer²²,
75 colon cancer²³, and pancreatic cancer^{24,25}. Multiple mechanisms have been proposed for triptolide-
76 induced antitumor activity, including inhibition of NF- κ B²⁶, and HSP70²⁷. Notably, Titov *et al.* reported
77 that triptolide binds covalently to human XPB (ERCC3) and inhibits its DNA-dependent ATPase
78 activity, leading to the inhibition of RNA polymerase II-mediated transcription and nucleotide excision

79 repair²⁸. However, it is unclear how this non-specific inhibition of an essential transcription factor
80 could exert selectivity against tumors.

81 While triptolide is a promising anti-cancer drug, poor solubility and toxicity have limited its
82 clinical development, and a number of analogs of triptolide have been developed for improved clinical
83 performance^{29,30}. In Phase I clinical studies, a soluble analog PG490-88/F60008³¹ resulted in
84 significant toxicity and had high interindividual variability in pharmacokinetic studies, thus stopping
85 further development. Minnelide³² is another analog with superior solubility and potent anti-tumor
86 activity in multiple preclinical cancer models. Phase I clinical trial (ClinicalTrials.gov Identifier:
87 NCT03129139) showed significant activity in highly refractory metastatic pancreatic cancer, and it is
88 currently in a Phase II open label trial (ClinicalTrials.gov ID NCT03117920).

89 In this study, we synthesized a novel pro-drug of triptolide, CK21, by decorating the C-19 with
90 a C-C double bond to generate (*E*)-19-[(1'-benzoyloxy-1'-phenyl)-methylidene]-Triptolide, formulated
91 it into an emulsion, and investigated its efficacy and mode of action. We report that CK21 inhibited the
92 *in vitro* proliferation of multiple pancreatic cancer cell lines, was effective at eliminating large
93 pancreatic tumors in heterotopic and orthotopic xenograft animal models with minimal toxicity, and
94 confirmed the efficacy of CK21 against multiple patient-derived pancreatic tumor organoids *in vitro*
95 and *in vivo*. We performed transcriptome analysis on the pancreatic organoid response to CK21 *in*
96 *vitro*, and on the *in vivo* response of pancreatic tumors to CK21. We identified that CK21 reducing
97 overall transcription, inhibited the NF- κ B pathway, induced mitochondria dysfunction, and ultimately,
98 mitochondrial-mediated apoptosis was identified as the likely mechanism for the anti-tumor activity of
99 CK21.

Results

Novel modified triptolide, CK21, show improved pharmacokinetics

We designed a new modification strategy to triptolide to generate CK21, by decorating the C-19 with a C-C double bond to generate (*E*)-19-[(1'-benzoyloxy-1'-phenyl)-methylidene]-Triptolide (Fig1.a). Briefly, a mixture of triptolide (1.8 g, 5 mmol) with anhydrous tetrahydrofuran (250 mL) was kept at -25°C~-20°C under nitrogen protection. Benzoyl chloride (1.05 mL, 7.5 mmol) and Lithium 2,2,6,6-tetramethylpiperidine in tetrahydrofuran/toluene (7.5mL, 2.0M, 15mmol) were then added dropwise to produce an intermediate compound, IM464. After 1 h, addition of benzoyl chloride and lithium 2,2,6,6-tetramethylpiperidine was repeated, and the reaction was quenched by adding aqueous sodium carbonate (6%). Following concentration under reduced pressure, the crude product was separated and purified by silica gel chromatography, and the target product collected and further recrystallized in methylene chloride/hexane to obtain CK21 that was used in the *in vitro* studies. Using ¹H NMR, ¹³C NMR and mass spectrometry, we confirmed the structure of CK21, and the absolute configuration of CK21 was established by single crystal X-ray diffraction (Fig1.b). We then formulated CK21 with medium chain triglycerides, phospholipids, glycerol, and DSPE-MPEG2000 (Fig1.c) to produce a CK21 emulsion (Fig1.d) that was used in the *in vivo* studies.

To examine the conversion of CK21 into triptolide *in vivo*, and to establish pharmacokinetics and to avoid toxicity, we intravenously administrated 3 mg/kg or 1.5 mg/kg CK21 into Sprague Dawley male or female rats, and the concentration of CK21 and triptolide in the plasma quantified. CK21 had a $T_{1/2}$ of 1.3 h and 0.225 h for male and female rats respectively. Released triptolide reached T_{max} at 0.25 and 0.75 h with a C_{max} of 78.3 and 81.9 nM respectively for male and female rats. A stable release of triptolide 30 nM to 80 nM was observed for up to 2 hours and undetectable after 4 hours (Fig.1e), and we hypothesized may mitigate the toxicity observed with other triptolide derivatives, which exhibit a spike release³¹. The maximum tolerated dose (MTD) of CK21 was 3 mg/kg/dose for female rats and 6 mg/kg/dose for male rats (Figure 1-source data1). Finally, we

125 observed that *in vitro* incubation of the human pancreatic cancer cell lines, AsPC-1, and Panc-1, with
126 CK21 at 5-100 nM for 24, 48 and 72 h resulted in a dose-and time-dependent inhibition of cell
127 proliferation (Fig.1f). When co-cultured with primary human fibroblast for 72 h, CK21 exhibited
128 significant toxicity only at 500 nM or higher (Figure 1-figure supplement 1).

129 A comparison of CK21 and triptolide (TP) revealed that they had similar IC50 (nM) when tested
130 *in vitro* using a cell viability assay with different cancer cell lines (Figure 1-source data 2). However,
131 the *in vivo* toxicity of TP in mice was significantly higher than CK21 *in vivo* (Figure 2-figure
132 supplement 1).

133 **CK21 inhibits AsPC-1 and Panc-1 proliferation *in vitro* and tumor growth *in vivo***

134 To evaluate the efficacy of CK21 pro-drug *in vivo*, we developed a xenograft model where
135 AsPC-1 tumors were subcutaneously implanted into female nude mice (Fig.2a). Daily treatment with
136 CK21 at all doses tested (1.25, 2.5, 3 and 5 mg/kg) significantly inhibited AsPC-1 tumor growth
137 (Fig.2c). Higher dosages of CK21 at 3 mg/kg or 5 mg/kg daily eliminated the tumor after 28 days of
138 treatment (Fig.2b). After 28 days of CK21 treatment, no mice from 3 mg/kg or 5 mg/kg groups
139 demonstrated tumor relapse during the subsequent 6-month follow-up observation (Figure 2-figure
140 supplement 2).

141 No significant weight loss was detected when female mice were treated with ≤ 3 mg/kg CK21,
142 compared to the control (no treatment) group (Fig.2d). In contrast, mice exhibited severe weight loss
143 with 5 mg/kg CK21. To further confirm the lack of toxicity of CK21 (3 mg/kg), we performed H&E
144 staining on the kidney, liver, and pancreas of mice after 28 days treatment. We did not observe any
145 evidence of toxicity, as the kidney, liver, and pancreas tissues appeared normal after 28 days of
146 CK21 treatment (Fig.2e); in contrast, after 14 days of CK21 treatment, AsPC-1 tumors showed a 5-
147 fold increase of TUNEL-positive staining compared to the no Rx group (Figs.2f&g). Thus, we
148 concluded that CK21 given at 3 mg/kg daily exhibited high efficacy and minimal toxicity, and this dose
149

150 was employed for the remaining of study. In a second subcutaneous xenograft model with the Panc-1
151 tumor cell line, 3 mg/kg daily of CK21 also resulted in significant inhibition of tumor growth (Figure 2-
152 figure supplement 3).

153 Orthotopic tumor mouse models are generally preferred over heterotopic subcutaneously-
154 located pancreatic tumors because they offer tissue site-specific pathology, allow studies of
155 metastasis, and are deemed more clinically relevant³³, while the development of pancreatic tumors
156 expressing luciferase/fluorescent proteins has facilitated the longitudinal monitoring of orthotopically
157 located pancreatic tumors³⁴. We next evaluated the efficacy of CK21 in an orthotropic xenograft
158 model, using luciferase-transfected AsPC-1 implanted into the pancreas of nude mice and allowing
159 the tumor to develop for 1-2 weeks before initiating CK21 treatment. The presence and size of the
160 tumor were monitored weekly by quantifying the bioluminescence intensity (Fig.2h), and overall, a 10
161 to 15-fold reduction in bioluminescence intensity was observed in mice that received CK21 compared
162 to untreated controls (Fig.2i). In addition, no mice died in the CK21 treatment group, whereas 5 out of
163 11 animals were sacrificed in the no Rx group due to the large tumor size (Fig.2j). Finally, we noted
164 that while most of the untreated mice develop metastatic disease by the end of the experiment
165 (Fig.2h), the CK21 treated mice did not. After 4 weeks of treatment, mice were monitored up to 3
166 months. All mice relapsed eventually in contrast to subcutaneous AsPC-1 tumors.

168 **Delayed CK21 therapy inhibits growth of tumors that escaped earlier therapies.**

169 The mortality of pancreatic tumors is often due to late detection when the tumor is at an
170 advanced stage. To evaluate the efficacy of CK21 against late-stage tumors, CK21 treatment was
171 initiated only after subcutaneous AsPC-1 tumors reached a large size of $\sim 900 \text{ mm}^2$ (Fig.3a). Despite
172 this delay in the initiation of treatment, CK21 was able to completely reduce the size of AsPC-1
173 tumors after 28 days of treatment, with all mice showing a significant response (Fig.3b).

174 Gemcitabine is a standard of care medication for pancreatic cancer in the clinic², therefore we
175 next tested whether gemcitabine in combination with CK21 might offer improved efficacy. We treated
176 mice for 4 weeks with suboptimal doses of CK21 (3 mg/kg, 3 days/wk) and gemcitabine (25 mg/kg, 3
177 days/wk), with each drug given on alternate days to avoid toxicity (Fig.3c). The combination therapy
178 did not show improved inhibition of AsPC-1 growth compared to CK21 monotherapy (Fig.3d) and
179 failed to induce complete regression of AsPC-1 tumors. In mice where tumors were detectable after
180 28 days treatment with CK21 or gemcitabine monotherapy, or combination therapy, we tested
181 whether switching to CK21 (3 mg/kg) daily treatment (Fig.3e) was able to induce tumor regression.
182 We observed that irrespective of whether mice failed CK21 (3x/wk) or gemcitabine monotherapy, or
183 combination therapy, switching to daily CK21 monotherapy for 28 days induced significant tumor
184 regression (Fig.3e).

185 186 **Transcriptome analysis of patient-derived organoids revealed early down-regulation of DDIT4** 187 **and XBP1 by CK21**

188 It is now recognized that 3-D patient-derived organoids offer a better recapitulation of the
189 heterogeneous, architectural, morphologic and genetic features of patient pancreatic tumor,
190 compared to long-term established 2-D monolayer cell lines³⁵⁻³⁸. We therefore investigated four
191 organoids derived from different pancreatic cancer patients³⁹, UC12-0118-8, U049MAI, U123SOK,
192 and U123M15-T, and tested the susceptibility to CK21 *in vitro* and *in vivo*. Details of the origin,
193 mutations of these organoids were described in Figure 4-source data 1. We observed that 72 hours of
194 *in vitro* incubation with CK21 (25 nM) significantly inhibited UC12-0118-8, U049MAI, and U123SOK
195 growth, and CK21 (50 nM) significantly inhibited proliferation of all four organoids (Fig.4a). In addition,
196 we were able to propagate U049MAI as a slow-growing subcutaneous tumor in nude mice. Treatment
197 with CK21 (3 mg/kg, daily) for 28 days, also significantly reduced U049MAI tumor growth compared
198 to the untreated control group (Fig.4b).

199 Because pancreatic tumor organoids better preserve the genetic signatures than pancreatic
200 tumor cell lines, we performed a time-course RNA-seq of U049MAI and U123M15-T treated with
201 CK21 for 3, 6, 9 and 12 hours. We hypothesized that these early time points might reveal the initiating
202 mechanism of action that result ultimately in the control of tumor growth; indeed, the number of
203 differentially expressed genes (DEGs) significantly increased with prolonged CK21 treatment, from
204 less than 10 DEGs at 3 h up to 8,000 DEGs at 12 h (Fig.4c & Figure 4-figure supplement 1). We
205 identified the genes that were differentially expressed at early time points and continuously
206 upregulated or downregulated at later time points (Fig.4d), and confirmed with qPCR, of a significant
207 downregulation of DDIT4, MYC, XBP1 and XIAP, as well as a significant upregulation of POLR2A,
208 GADD45 and VAMP1 (Fig.4e). We also performed transcriptome analysis on the AsPC-1 tumor,
209 orthotopically implanted in the pancreas for 7 days and then treated by CK21 for three days. Notably,
210 CK21 induced similar DEG expression profiles as *in vitro* treated organoids, with downregulated
211 DDIT4 and XBP1, as well as upregulated POLR2A (Fig.4g).

212 DDIT4 was one of the genes consistently and strongly downregulated by CK21 in both
213 organoids and AsPC-1, with significant effects observed as early as 3 hours of CK21 treatment *in*
214 *vitro* and at day 3 *in vivo*. At the protein level, we also observed a significant decrease of DDIT4
215 expression after CK21 treatment of 24 hours (Figure 4-figure supplement 2). Interestingly, DDIT4 has
216 been identified as a prognosis marker and highly expressed in pancreatic tumors⁴⁰, thus prompting
217 the investigation into whether DDIT4 inhibition might be the triggering mechanism of action and thus
218 serve as a predictive biomarker for CK21 sensitivity. However, knock-down of DDIT4 in Panc-1 only
219 induced very modest *in vitro* susceptibility to CK21, and the overexpression of DDIT4 in AsPC-1 didn't
220 result a difference to CK21 response (Figure 4-figure supplement 3). Furthermore, in two mouse
221 pancreatic tumor cell lines derived from genetically modified KC or KPC mice that were only modestly
222 sensitive to CK21 treatment (Figure 4-figure supplement 4), DDIT4 as well as other early responder
223 genes showed strong alterations in expression profiles comparable to tumors that were more

224 sensitive to CK21 (Figure 4-figure supplement 5). Therefore, these early responder genes are not
225 likely to be essential mediators leading to tumor susceptibility to CK21.

226 227 **Ingenuity pathway analysis of patient-derived organoids reveal down-regulation of the NF- κ B** 228 **signaling pathway by CK21**

229 At the later timepoint of 12 h after CK21 treatment, both U049MAI and U123M15-T had over
230 8,000 DEGs compared to the no Rx group (Figs.5a&b). We then used Ingenuity pathway analysis
231 (IPA, Qiagen) on the DEGs to identify the major molecular and cellular functions that were
232 significantly affected by CK21 treatment (Fig.5c). First, CK21 treatment was predicted to inhibit RNA
233 and DNA transcription, expression of RNA, and transactivation of RNA transcription in both organoids;
234 this observation corroborates a previous report on the ability of triptolide to inhibit RNA transcription²⁸.
235 In addition, DEGs induced by CK21 were enriched for inhibition of cell proliferation and cell survival,
236 and for inducing apoptosis and tumor cell necrosis. These observations collectively are consistent
237 with TUNEL-positive staining of ASPC-1 with CK21 treatment *in vivo*, and support the conclusion that
238 induction of cell apoptosis is the likely mechanism for the anti-tumor activity of CK21.

239 We used IPA pathway enrichment analysis to further identify the canonical signaling/metabolic
240 pathways regulated by CK21 that might lead to tumor cell apoptosis (Figs.5d&e). Interestingly, in both
241 organoids, EIF2 signaling, oxidative phosphorylation and mitochondrial dysfunction were the major
242 pathways highly upregulated by CK21, whereas the NF- κ B, TGF- β and telomerase signaling
243 pathways were significantly downregulated at the 12 h treatment timepoint. In addition, at 9-hour
244 timepoint, NF- κ B was already significantly downregulated and oxidative phosphorylation as well as
245 EIF2 signaling pathway were significantly upregulated (Figure 5-figure supplement 1). *In vivo*, Aspc-1
246 orthotopic tumors showed upregulation of DNA damage checkpoint regulation (Figure 5-figure
247 supplement 2), which also is an indicator of tumor apoptosis. Collectively, these observations suggest
248 that CK21 may be inhibiting NF- κ B activity and inducing mitochondrial-mediated tumor cell apoptosis.

249

250 **CK21 inhibits expression of NF- κ B p65 and translocation to nuclei**

251 NF- κ B plays a major role in the regulation of immune, inflammatory response and cell
252 proliferation⁴¹. In normal cells, NF- κ B is activated by appropriate stimuli and then returns to its
253 inactive state. In tumor cells, particularly in pancreatic cancer cells, NF- κ B becomes constitutively
254 activated and has an anti-apoptotic function^{42,43}. After 12 h treatment with CK21, the genes (CHUK,
255 IKBKB and RELA) encoding the key regulators of the NF- κ B pathway, IKK α , IKK β and p65, were
256 significantly downregulated in both organoids (Fig.6a).

257 To confirm the transcriptional findings that CK21 downregulates the NF- κ B pathway, we
258 stained the nuclei and p65 of AsPC-1 and Panc-1 with different fluorophores to visually determine
259 their cellular location; similarity in the spatial localization between p65 and nuclei represents the
260 translocation of NF- κ B to nuclei (Fig.6b). In the no Rx group, p65 staining had a high similarity with
261 nuclei staining, corresponding with constitutive nuclear localization of NF- κ B in pancreatic cancer
262 cells. After treatment with CK21 for 24 or 48 hours, both cell lines exhibited significantly lower
263 expression of p65, consistent with RNA-seq analysis (Fig.6c). In addition, we observed reduced
264 similarity of p65 and nuclei, indicating significantly reduced translocation of NF- κ B to the nuclei in the
265 presence of CK21 (Figs.6d&e). Taken together, the data demonstrate that CK21 inhibits NF- κ B
266 expression and translocation, which we hypothesize results in increased susceptibility tumor cell
267 apoptosis.

268

269 **CK21 induces reactive oxidative species and mitochondrial mediated apoptosis**

270 The expression of genes encoding five mitochondrial respiratory chain complexes were
271 significantly increased in pancreatic tumor organoids treated with CK21(Fig.6f), consistent with
272 dysregulated mitochondrial function and increased susceptibility to mitochondrial-mediated
273 apoptosis⁴⁴. Because mitochondrial mediated apoptosis is often stimulated by oxidative stress, we

274 first tested whether CK21 induced reactive oxidative species (ROS) in AsPC-1 and Panc-1 pancreatic
275 tumor cell lines. In both cell lines, a trend towards an increase in ROS was observed as early as 8
276 hours after CK21 treatment, and a significant increase in ROS generation after 24 hours of culture
277 with CK21 (Fig.6g). These observations raise the possibility that increased ROS production may
278 trigger mitochondrial outer membrane permeabilization and release of pro-apoptotic mitochondrial
279 proteins into the cytoplasm⁴⁴.

280 The B-cell-lymphoma protein 2 (BCL2) family of proteins also play critical roles in regulating
281 the mitochondrial pathway of apoptosis, and BCL2 functions as a critical anti-apoptotic survival
282 protein⁴⁵. To test whether BCL2 protein is reduced in CK21-treated cells, we quantified BCL2 protein
283 expression by Western blotting. We observed that BCL2 was significant decreased in both AsPC-1
284 and Panc-1 cell lines, and in U049MAI, after 24 hours of CK21 culture (Fig.6h).

285 Because most apoptotic pathways lead to the activation of cysteine-dependent aspartate-
286 specific proteases, and ultimately to cleaved effector caspases such as caspases-3, -6 and -7⁴⁵, we
287 probed for cleaved caspase-3 in pancreatic tumors incubated with CK21. For Panc-1 and both
288 pancreatic tumor organoids, cleaved caspase-3 was detected after 24 hours of culture with CK21
289 (Fig.6i) by Western blotting. We also confirmed increased caspase-3/7 in Panc-1 by flow cytometry
290 (Figure 6-figure supplement 1). Interesting, cleaved caspase-3/7 was not detected in AsPC-1 after
291 CK21 treatment, suggesting that apoptosis of these tumor cells may be explained by the involvement
292 of other effector caspases or proteases. Collectively, these data point to CK21 downregulating the
293 NF-kB pathway, promoting ROS production and mitochondrial-mediated tumor cell apoptosis.

294 295 **CK21 showed minimal immunosuppression in a spontaneous tumor rejection model**

296 A number of studies have reported on the immunosuppressive activity of triptolide⁴⁶, thus
297 raising the potential concern that CK21 may also inhibit the development of anti-tumor immune
298 responses and prevent long-term tumor control. Indeed, although the analyses were conducted on

299 CK21 treated tumor cells, IPA analysis indicated that CK21 inhibited lymphopoiesis, leukopoiesis and
300 T cell development, consistent with potential immunosuppressive activity. To address this concern,
301 we utilized a mouse KPC-960 pancreatic ductal-like tumor model derived from pancreatic tumors that
302 spontaneously arose in KPC (*Kras*^{G12D/+} *Trp53*^{R172H/+} *Pdx1-Cre*) B6.129 mice⁴⁷ (Fig.7a). Upon
303 subcutaneous implantation into B6.129 immunocompetent hosts, KPC-960 grew to a maximum tumor
304 size by day 7 and then approximately 70% KPC-960 tumors were spontaneously rejected by day 14-
305 17 post-implantation (Fig.7b). This contrasted with tumor formation in similar B6.129 host in Torres et
306 al.⁴⁷; we speculate that rejection of the KPC-960 tumor may be driven increased number of passages
307 that resulted in the accumulation of mutations and/or to antigenic drift. To test whether CK21 could
308 prevent the spontaneous regression of KPC-960, CK21 (3 mg/kg daily) therapy was initiated on day 5
309 or 7 post-implantation. We observed no statistically significant inhibition of tumor regression when
310 CK21 treatment was started on day 5 or 7 post-implantation (Figs.7c&d) suggesting that the
311 immunosuppressive activity of CK21 on established primary immune responses is minimal. We also
312 implanted KPC-960 subcutaneously into nude mice and observed limited efficacy of CK21 when
313 provided at 3 mg/kg/day (Figure 7-figure supplement 1). These observations suggest that host
314 immunity is primary responsible for the rejection of KPC-960 tumors. The reason for the resistance to
315 CK21 is not known and is the subject of future investigations.

316 We next tested the possibility that CK21 may have inhibited the development of memory and
317 recall anti-tumor responses that mediate the spontaneous rejection of secondary KPC-960 tumors.
318 Mice that cleared these tumors were rested for 2 weeks without treatment and then challenged with a
319 second KPC-960 tumor (Fig.7a); a more rapid tumor clearance was observed (Fig.7e). When CK21
320 treatment was initiated on day 3 of second tumor implantation, no significant change in the kinetics of
321 tumor regression was observed compared to untreated controls (Fig.7f). In addition, mice that
322 rejected the first KPC-960 tumors while receiving CK21 were rested and re-challenged with a second
323 KPC-960 tumor. All the mice were able to reject the tumor comparably to those that did not receive

324 CK21, (Fig.7g). These observations further demonstrate CK21 did not inhibit the development of
325 memory or recall anti-tumor responses.

326 Finally, to evaluate the quality of tumor-specific T cells after CK21 treatment, we performed an
327 *ex vivo* tumor killing assay. Splenocytes were harvested from untreated mice that had rejected tumors,
328 or mice that had received CK21-treatment after 1° or 2° tumor implantation and cultured with KPC-
329 960 or a control KPC-6141 tumor *ex vivo* (Fig.7h). Splenocytes from mice treated with CK21 exhibited
330 comparable killing of KPC-960 as splenocytes from untreated mice (Fig.7i). Collectively these data
331 suggest that despite potent anti-tumor activity, CK21 was minimally immunosuppressive.

332 Discussion

333 Toxicity is the key challenge for using triptolide and its derivatives for its use as an anti-tumor
334 agent in the clinic. Hepatotoxicity, reproductive toxicity, and nephrotoxicity have been identified as the
335 major side effects for triptolide⁴⁸. In addition, sex differences have been observed, where the female
336 rats showed more toxicity under the same dosage of triptolide⁴⁹. Cytochrome P450s (CYP) is
337 essential for the metabolism of triptolide and CYP3A2, a male-predominant form in rats, may
338 contribute to the sex-related differences⁵⁰. Similar sex differences were also observed for CK21,
339 where half the dose of CK21 in female rats had a similar triptolide exposure in plasma as male rats
340 (Fig.1e), and the maximum tolerated dose of CK21 was 3 mg/kg/dose for female rats and 6
341 mg/kg/dose for male rats (Figure 1-source data1). Consistent with the MTD of CK21 being different
342 for male/female rats, we observed comparable efficacy of CK21 at 3 mg/kg in female mice (Fig.2c),
343 and at 1.5 mg/kg in male mice (Figure 2-figure supplement 4). Whether these sex difference in
344 triptolide metabolism will affect dosing in the clinic will have to be investigated in Phase I clinical trials.
345 Nevertheless, despite sex difference, stable exposure of triptolide upon conversion from CK21
346 resulted in significantly mitigated toxicity, compared to other analogs such as F60008 that showed a
347 steep release of triptolide which, we speculate, would lead to triptolide overexposure and severe
348 toxicity observed in Phase 1 trials³¹. Another triptolide analog, MRx102 had a MTD of 3 mg/kg/dose

349 for the female rats and 4.5 mg/kg/dose for the male rats⁵¹. Thus, under the pharmacokinetic profile of
350 CK21, we were able to dose the female athymic nude mice up to 5 mg/kg/day for 28 days with
351 tolerable weight loss (Fig.2d), and at 3 mg/kg/day, where CK21 showed potent efficacy and no
352 obvious toxicity (Figs.2c-e).

353 We used rigorous time-course transcriptomic profiling of pancreatic tumors response to CK21
354 to identify its mechanism of action on patient-derived pancreatic tumor organoids. Overall, the effect
355 of CK21 corresponded to the major reported anti-tumor functions of triptolide, namely transcription
356 inhibition and apoptosis induction. Triptolide was reported by Tivov *et al.* to covalently bind to XPB, a
357 subunit of the transcription factor TFIIH, resulting in the inhibition of its DNA-dependent ATPase
358 activity, RNA polymerase II (Pol II)-mediated transcription and likely nucleotide excision repair²⁸.
359 Chen *et al.* further confirmed that triptolide functioned as a XPB/TFIIH inhibitor to limit promoter-
360 proximal Pol II transcription initiation, resulting in decreased Pol II levels as early as 2 hours of
361 treatment⁵². Likewise, our transcriptome analyses revealed broad downregulation of transcription and
362 transactivation of RNA after 12 h CK21 treatment (Fig.5c). Furthermore, as early as 6 h of treatment,
363 we observed a significant downregulation of critical transcription factors, including XBP1 and ZNF628
364 (Fig.4d), which may mediate the broad inhibition of RNA and DNA transcription, as well as of RNA
365 transactivation and expression, observed at 12 h post-CK21 treatment (Fig.5c). Inhibition of RNA
366 transcription and blockade of RNA synthesis can potentially lead to programmed cell death. For
367 example, Santo *et al.* used a cyclin-dependent kinase inhibitor to inhibit Pol II phosphorylation and
368 observed induction of apoptosis in myeloma cells⁵³. Cai *et al.* also suggested inhibition of Pol II
369 expression and phosphorylation resulted reduced expression of Mcl-1 and X-linked inhibitors of
370 apoptosis (XIAP)⁵⁴. Similarly, Carter *et al.* reported that tumor cell apoptosis induced by triptolide was
371 accompanied by decrease of XIAP levels¹⁸. Consistent with Carter *et al.* we also observed a
372 significant decrease of XIAP expression after CK21 treatment of two human pancreatic organoids *in*
373 *vitro*, and of orthotopically transplanted AsPC-1 tumors *in vivo* (Figs.4d, f, g).

374 Our analysis of enriched signaling/metabolic pathways (Figs.5d&e) predicted the downstream
375 effects of CK21 inhibition of general transcription might lead to tumor cell apoptosis. As a potential
376 consequence of transcription inhibition, genes for the key regulators of NF- κ B pathway, such as
377 CHUK, IKBKB and RELA, were significantly downregulated in both organoids (Fig.6a& Figure 6-figure
378 supplement 2). We also observed decreased p65 expression at a protein level and reduced
379 translocation of the NF- κ B complex to the nucleus (Figs.6b-e). Therefore, activation of the NF- κ B
380 pathway was significantly inhibited after treatment with CK21. In addition to promoting cell
381 proliferation and immune responses⁴¹, NF- κ B also plays a role in controlling mitochondrial dynamics
382 and cell apoptosis⁵⁵. Pazarentzos *et al.* demonstrated the localization of I κ B α on the outer membrane
383 of mitochondrial functions to inhibit apoptosis, especially in the tumor cells⁵⁶. Liu *et al.* indicated the
384 inhibition of NF- κ B alone can induce the release of cytochrome C from mitochondria⁵⁷. In our study,
385 we observed a significant downregulation of NFKBIA, which encodes I κ B α , in both organoids after
386 CK21 treatment (Fig.6a& Figure 6-figure supplement 2). In addition, we also observed that the
387 expression of genes encoding five mitochondrial respiratory chain complexes was significantly
388 increased in pancreatic tumor organoids treated with CK21(Fig.6f). Collectively these data suggest a
389 downstream effect of CK21 inhibition of NF- κ B is the promotion of dysregulated mitochondrial
390 function and subsequently, increased susceptibility to mitochondrial-mediated intrinsic apoptosis⁴⁴.
391 Nevertheless, we cannot exclude the possibility that the changes in gene expression could reflect
392 different stability of mRNA, and not directly related to the CK21 modifying general transcription.

393 As upstream regulators, BCL2 family proteins that reside or congregate on the surface of
394 mitochondria govern cell-intrinsic apoptosis⁵⁸. BCL2 family proteins have opposing functions in
395 regulating the equilibrium of mitochondrial membrane potential: BCL2 is anti-apoptotic and promotes
396 cell proliferation⁵⁹ whereas BAX is pro-apoptotic^{60,61,62}. Under CK21 treatment, BCL2 expression in
397 pancreatic cancer cells was significantly reduced (Fig.6h). Similar observations were reported in
398 leukemic cells¹⁸ and melanoma cells⁶³ after treated with triptolide. Thus CK21 may tip such

399 equilibrium towards permeabilization and release of apoptogenic molecules into cytoplasm⁶².
400 Eventually, effector caspases, such as caspase 3, 6, and 7, are cleaved and activated to induce
401 apoptosis. In our study, we observed a significant increase of cleaved caspase 3 for Panc-1 and both
402 pancreatic tumor organoids (Fig.6i). Finally, we noted subtle differences in the extent to which Bcl2 is
403 inhibited and Caspase 3 is activated following CK21 treatment of the two pancreatic tumor cell lines
404 and two patient-derived organoids; these observations underscore the notion that broad inhibition of
405 RNA transcription allows CK21 to leverage distinct vulnerabilities and pathways to achieve apoptosis
406 in different tumor cells.

407 Taken together, our study describes the development of a novel modified triptolide, CK21, with
408 improved pharmacokinetics, and efficacy for pancreatic tumor cell lines and patient-derived
409 pancreatic tumor organoids. Transcriptomic profiling of the organoids and verification of protein
410 expression collectively point to the induction of tumor cell apoptosis by CK21 is mediated by the
411 inhibition of general transcription, leading to downstream effects involving NF- κ B inhibition and
412 mitochondria dysfunction.

Key Resources Table

Reagent type (species) or resource	Designation	Source or reference	Identifiers	Additional information
Chemical compound, drug	CK21	In house	NA	
Chemical compound, drug	Gemcitabine	Actavis	45963-619-59	
Cell line (Homo-sapiens)	AsPC-1	ATCC	CRL-1682™	
Cell line (Homo-sapiens)	Luciferase transfected AsPC-1	Indiana University	N/A	Luciferase transfected
Cell line (Homo-sapiens)	Panc-1	ATCC	CRL-1469™	
Cell line (Mus)	KC-6141	University of Nebraska	N/A	
Cell line (Mus)	KPC-960	University of Nebraska	N/A	
Cell line (Mus)	KPC-961	University of Nebraska	N/A	
Biological sample (Mus)	B6129SF1/J	Jackson Laboratory	101043	
Biological sample (Mus)	C57BL/6J	Jackson Laboratory	000664	
Biological sample (Mus)	Athymic Nude-Foxn1 ^{nu}	Envigo		
Commercial assay or kit	DMEM	ATCC	30-2002™	
Commercial assay or kit	RPMI	Quality Biological	112-024-101	
Commercial assay or kit	Fetal bovine serum	Atlanta Biologicals	S115OH	
Commercial assay or kit	Penicillin streptomycin	Gibco	15140-122	
Commercial assay or kit	L-Glutamine	Gibco	25030-081	
Commercial assay or kit	DMSO	Sigma	276855	
Commercial assay or kit	Trypsin-EDTA	Stemcell	07901	
Commercial assay or kit	TrypLE™ express	Gibco	12605-010	
Commercial assay or kit	Sodium pyruvate	Gibco	11360-070	
Commercial assay or kit	MEM nonessential amino acids	Cellgro	25-025-CL	
Commercial assay or kit	2-Mercaptoethanol	Gibco	21985-023	
Commercial assay or kit	IntestiCult™ organoid growth medium	Stemcell	6005	
Commercial assay or kit	A83-01	Sigma	SML0788	
Commercial assay or kit	FGF-10	Sigma	SRP3262	
Commercial assay or kit	Gastrin I	Sigma	G9145	
Commercial assay or kit	N-acetylcysteine	Sigma	A9165	
Commercial assay or kit	Nicotinamide	Sigma	N0636	
Commercial assay or kit	B27 supplement	Gibco	17504-044	
Commercial assay or kit	Primocine	Invivogen	ant-pm-1	
Commercial assay or kit	Y-27632	Tocris	1254	
Commercial assay or kit	Matrigel	Corning	356231	
Commercial assay or kit	TrypLE™	Gibco	12605-010	
Commercial assay or kit	CellTiter 96® AQueous one solution	Promega	G3580	
Commercial assay or kit	Caspase-3/7 green detection	Thermo Fisher	C10427	
Commercial assay or kit	SYTOX® dead cell stain	Thermo Fisher	C10427	

Commercial assay or kit	CFSE cell proliferation kit	Thermo Fisher	C34554	
Commercial assay or kit	ACK lysing buffer	Quality Biological	118-156-101	
Commercial assay or kit	ROS-Glo™ H ₂ O ₂ assay	Promega	G8820	
Commercial assay or kit	NuPAGE™ 10% Bis-Tris gel	Invitrogen	NP0301BOX	
Commercial assay or kit	NuPAGE® MES SDS running buffer	Novex	NP002	
Commercial assay or kit	NuPAGE® MOPS SDS running buffer	Novex	NP001	
Commercial assay or kit	NuPAGE® transfer buffer	Novex	NP0006-1	
Commercial assay or kit	NuPAGE® LDS sample reducing agent	Invitrogen	NP0007	
Commercial assay or kit	NuPAGE® sample buffer	Invitrogen	NP0009	
Commercial assay or kit	NuPAGE™® antioxidant	Invitrogen	NP0005	
Commercial assay or kit	TBS Tween™-20 buffer	Thermo Scientific	28360	
Commercial assay or kit	Invitrolon™ PVDF filter paper	Novex	LC2005	
Commercial assay or kit	PageRuler prestained protein ladder	Thermo Scientific	26616	
Commercial assay or kit	Methanol	Fisher Scientific	A452-4	
Commercial assay or kit	Pierce™ protease&phosphatase inhibitor	Thermo Scientific	A32959	
Commercial assay or kit	Bovine serum albumin	Sigma	A7906	
Commercial assay or kit	SuperSignal™ west pico PLUS	Thermo Scientific	34579	
Commercial assay or kit	Pierce™ bradford assay kit	Thermo Scientific	23246	
Antibody	Anti-beta actin (Rabbit polyclonal)	Abcam	ab8227	(1:2000)
Antibody	Recombinant anti-REDD-1/DDIT4 (Rabbit monoclonal)	Abcam	ab191871	(1:1000)
Antibody	Anti-Caspase-3 (Rabbit polyclonal)	Abcam	ab13847	(1:500)
Antibody	Recombinant anti- BCL2 (Rabbit monoclonal)	Abcam	ab182858	(1:2000)
Antibody	Goat anti-rabbit IgG H&L (Goat polyclonal)	Abcam	ab205718	(1:10000)
Antibody	Phospho-NFκB p65, PE, eBioscience™(Mouse monoclonal)	Invitrogen	12986342	(1:100)
Commercial assay or kit	4',6-Diamidino-2-Phenylindole, Dilactate	Biolegend	422801	(1:1000)
Commercial assay or kit	PowerUp™ SYBR™ green master mix	Applied Biosystem	A25742	
Commercial assay or kit	High capacity cDNA reverse transcription	Applied Biosystem	4368814	
Commercial assay or kit	D-Luciferin potassium salt	Perkin Elmer	122799	
Commercial assay or kit	PBS	GenClone	25-508	
Commercial assay or kit	Cell recovery solution	Corning	354253	
Commercial assay or kit	RNeasy® Plus Mini Kit	Qiagen	74124	
Commercial assay or kit	DNase I recombinant	Roche	04536282001	

417

418

Methods

419

Study design overview

420 We synthesized a novel pro-drug of triptolide, CK21, and formulated it into an emulsion. We
421 tested the efficacy of CK21 *in vitro* using cell proliferation assays and multiple pancreatic cancer cell
422 lines, and *in vivo* in heterotopic and orthotopic xenograft mouse models. We also tested the efficacy
423 of CK21 against multiple patient-derived pancreatic tumor organoids *in vitro* and *in vivo*. We
424 performed transcriptome analysis on the pancreatic organoid response to CK21 *in vitro*, and on the *in*
425 *vivo* response of pancreatic tumors to CK21. This analysis identified the ability of CK21 to reduce
426 overall transcription, inhibit the NF- κ B pathway, induce mitochondria dysfunction, and ultimately,
427 mitochondrial-mediated apoptosis. We confirmed inhibition of NF- κ B expression and translocation in
428 pancreatic cell lines using imaging flow cytometry, Western blotting and RT-PCR.

429

430 **Ethics statement and study approval**

431 All animal experiments were approved by the Institutional Animal Care and Use Committee at
432 the University of Chicago, and adhered to the standards of the NIH Guide for the Care and Use of
433 Laboratory Animals. Pancreatic tumors from patients with pancreatic ductal adenocarcinoma were
434 collected under University of Chicago IRB12-1108 and IRB13-1149.

435

436 **Reagents**

437 Human pancreatic tumor cell lines were obtained from commercial sources. Human tumor
438 organoids were obtained from patients with pancreatic ductal adenocarcinoma, confirmed to be tumor
439 based on pathologic assessment, and developed into organoid culture according to established
440 protocols³⁹. Luciferase-transfected AsPC-1 tumors³⁴, and mouse tumors from genetically KPC mice
441 that spontaneously develop pancreatic cancer⁴⁷ have been previously described. CK21 was
442 synthesized as described below. All other reagents listed in the Key Resources Table were validated
443 by the manufacturer.

444

445 **Synthesis and formulation of CK21**

446 Under nitrogen protection, a mixture of triptolide (1.8 g, 5 mmol) and anhydrous
447 tetrahydrofuran (250 mL) was cooled to -20 °C, and lithium 2,2,6,6-tetramethylpiperidine in
448 tetrahydrofuran/toluene (7.5 mL, 2.0M, 15 mmol) was added dropwise. After stirring for 30 min,
449 benzoyl chloride (1.05 mL, 7.5 mmol) was added dropwise and reacted for 1 h, followed again with
450 benzoyl chloride (7.5 mmol) and reacted for another 2 h. The reaction was quenched by adding
451 aqueous sodium carbonate (10%), and the mixture was extracted with ethyl acetate (250 mL×3). The
452 organic phases were combined, dried over anhydrous sodium sulfate, and concentrated under
453 reduced pressure. The crude product was separated and purified by silica gel chromatography
454 (dichloromethane: ethyl acetate = 2:1), and the target product (white solid, 2.55 g, yield 90%) was
455 collected and further recrystallized in a mixed organic solvent (dichloromethane/hexane) to obtain a
456 final product (2.13 g, yield 85%, purity >99% by UPLC).

457 CK21 was dissolved in medium chain triglycerides (MCT) at 90°C under nitrogen. PC-98T,
458 DSPE-MPEG2000 and glycerol were dissolved in water to form the water phase. The oil phase was
459 dispersed at room temperature in the water phase with high-speed shear mixing (FAS90-22, FLUKO)
460 at 2,800 rpm for 30 min. The pH was adjusted to 4-7, and volume was made up to 100% with water.
461 The final emulsion was obtained by high-pressure homogenization using microfluidizer (M-7125-20K,
462 MFIC) at 10,000 psi for one cycle and at 18,000 psi for two cycles. Finally, the emulsion was sealed
463 in vials (5 mL: 1.5 mg) after flushing with nitrogen gas and autoclaved at 121°C for 15 min.

464

465 **Characterization of CK21 compound**

466 ¹H NMR (Bruker, 400MHz, CDCl₃): δ 8.25 (dd, J = 1.6 Hz, 8.0 Hz, 2H), 7.76 (dd, J = 1.6 Hz,
467 8.4 Hz, 2H), 7.67 (m, 1H), 7.58 (t, J = 7.2 Hz, 2H), 7.43~7.38 (m, 3H), 3.80 (d, J = 3.2 Hz, 1H), 3.39
468 (d, J = 2.8 Hz, 1H), 2.98 (d, J = 10 Hz, 1H), 2.75~2.69 (m, 1H), 2.63~2.58 (m, 1H), 2.56 (d, J = 6.4 Hz,

1H), 2.53 (d, J = 10 Hz, 1H), 2.40~2.32 (m, 2H), 2.21~2.14 (m, 1H), 1.88 (dd, J = 14.0 Hz, 13.2 Hz, 1H), 1.55~1.52 (m, 1H), 1.18~1.11 (m, 1H), 1.15 (s, 3H), 0.92 (d, J = 7.2 Hz, 3H), 0.82 (d, J = 6.8 Hz, 3H); ¹³C NMR (Bruker, 100 MHz, CDCl₃): δ168.1, 164.5, 150.3, 142.2, 134.4, 133.5, 131.9, 130.5, 129.9, 129.2, 128.9, 128.6, 128.1, 128.0, 72.8, 65.8, 65.3, 60.7, 60.0, 56.5, 53.7, 40.7, 36.7, 29.3, 27.9, 24.6, 17.8, 17.6, 16.7, 15.0.

Mass Spectrometry (AGILENT, ESI+): Calculated for C₃₄H₃₂O₈[M]: 568.62, found 569.22 [M⁺H]⁺ and 591.21 [M⁺Na]⁺.

CK21 crystals were obtained by careful evaporation of a mixture of CK21 in combined solvent of dichloromethane and hexane at room temperature. A crystal with size of 0.10×0.03×0.02 mm was chosen to be scanned at X-ray diffraction. Data collection was carried out using a Bruker D8 Venture diffractometer with graphite mono-chromated Ga K α radiation (λ = 1.34139 Å) at 296 K. Structures were solved by direct methods using the SHELXS program and refined with the SHELXL program (Bruker).

Pharmacokinetic study of CK21

CK21 emulsion (0.3 mg/mL) was injected intravenously into fasted SD rats at a dose of 3 mg/kg for males and 1.5 mg/kg for females. At designed timepoints, 60 μ L blood samples were collected, protein precipitated and centrifuged at 13000 rpm for 10 min, 4°C. 5 μ L of the supernatant was injected for LC-MS/MS (Q-Trap 6500) analysis. The PK data were calculated using Phoenix WinNonlin 6.3.

Human pancreatic cancer cell lines and organoids

Human pancreatic cancer cell line, AsPC-1, was cultured in RPMI with 10% fetal bovine serum (FBS), 1% L- Glutamine, and 1% penicillin streptomycin(P/S). Panc-1 was cultured in DMEM with 10% FBS and 1% P/S. Both AsPC-1 and Panc-1 were purchased from ATCC.

494 Pancreatic tumors from patients with pancreatic ductal adenocarcinoma were collected under
495 IRB12-1108 and IRB13-1149, confirmed to be tumor based on pathologic assessment, and
496 developed into organoid culture according to established protocols³⁹. Four different organoids,
497 U0118-8, U049MAI, U114SOK, and U123M15-T, were investigated. For the optimal culture, derived
498 organoids were embedded in growth factor reduced Matrigel and cultured in Intesticult™ complete
499 media, supplemented with A83-01, fibroblast growth factor 10, gastrin I, N-acetyl-L-cysteine,
500 nicotinamide, and B27 supplement, primocin. Tocris Y-27632 dihydrochloride, a selective p160
501 ROCK inhibitor, was added when thawing the organoids³⁹.

502

503 ***In vitro* proliferation assay**

504 AsPC-1, Panc-1 and tumor organoids were seeded in 96-well plates and cultured with the
505 indicated concentrations of CK21, or Gemcitabine. CK21 was prepared by dissolving in DMSO and
506 diluting with PBS. At selected times, 20 μ L of CellTiter 96® AQueous One solution was added into
507 the 96-well plate, and then incubated at 37°C for 2 hours. The absorbance was read at 490 nm using
508 Spectra Max® i3X (Molecular Devices).

509

510 **Mice and xenograft**

511 All animal work that described in this study were approved by the Institutional Animal Care and
512 Use Committee (ACUP72467, ACUP72527). Female or male athymic nude-Foxn1^{nu} mice age from 6
513 to 8 weeks were purchased from Envigo. AsPC-1 or Panc-1 cells were subcutaneously implanted in
514 the scruff of a nude mice at 5×10^6 cells/mice. Mice were treated with different dosages of CK21 daily
515 by intraperitoneal injection. Blank emulsion was provided to the no treatment group. Gemcitabine was
516 also provided to mice at 75 mg/kg once a week as a positive control. The effect of CK21 with another
517 human pancreatic tumor cell line, Panc-1, was also evaluated in the subcutaneous model. The
518 U049MAI organoid was used to test the efficacy of CK21 in the same way.

519 Tumor size was recorded weekly and calculated by $1/2 \times L \times W^2$. L was the length of the tumor;
520 W was the width of the tumor. Weight of mice were monitored once a week. At the end of the
521 experiment, mice were sacrificed by cervical dislocation. Liver, kidney, pancreas, as well as tumor
522 tissue were harvested and fixed in 10% formalin. Haematoxylin and Eosin (H&E), terminal
523 deoxynucleotidyl transferase dUTP nick end labeling (TUNEL) staining were performed on respective
524 tissues. All the slides were scanned using ScanScope XT slide scanner and analyzed using Aperio
525 eSlideManager.

527 **Orthotopic Tumor Model with Transfected AsPC-1**

528 Luciferase-transfected AsPC-1³⁴ (1×10^6 /mouse) was injected into the tail of the pancreas, and
529 one week of tumor implantation, CK21 was provided at 3 mg/kg daily for the treatment group. In the
530 no treatment group, blank emulsion was provided. During the four weeks of treatment, mice were
531 administrated with D-luciferin (Perkin Elmer) and subjected to Xenogen bioluminescence imaging
532 weekly.

534 **Immunomodulation of CK21 at a spontaneous rejection mice model**

535 Murine pancreatic cancer cell lines were derived from KPC (*Kras*^{G12D};*Trp53*^{R172H};*Pdx1-Cre*)
536 mice or KC (*Kras*^{G12D};*Pdx1-Cre*) mice, which spontaneously develop pancreatic cancer⁴⁷. KPC-960
537 were developed from KPC mice with a mixed background of B6×129, and were subcutaneously
538 implanted into female, naïve B6×129 mice at 5×10^6 cells/mice. After spontaneous rejection, mice
539 were rested for 2 weeks and then challenged with KPC-960 cells at 5×10^6 cells/mice. A dosage of 3
540 mg/kg of CK21 was provided daily starting at day 5 or day 7. For evaluation of CK21 on memory
541 response, mice that rejected the tumors without any CK21 treatment were rested for 2 weeks and
542 then received a second tumor challenge and 3 mg/kg of CK21 daily, starting at day 3.

543 Mice that rejected the KPC-960 tumor were sacrificed, splenocytes were collected and ex-vivo
544 specific cytotoxic assay performed. Specifically, target cells KPC-960 and negative control KC-6141
545 were labeled at 10:1 concentration of carboxyfluorescein succinimidyl ester (CFSE) respectively. Two
546 cell lines were then mix at 1:1 ratio and cultured with harvested splenocytes at 1:1, 1:5, 1:10, 1:20,
547 and 1:50 ratios. After overnight co-culture, cells were subjected to flow cytometry (BD™ LSR II) to
548 quantify relative cytotoxicity.

549 **Transcriptome analysis of CK21 treated patient-derived organoids**

550 Two organoids, U049MAI, U123M15-T, were cultured with CK21 at 50 nM for 3 hours, 6 hours,
551 9 hours and 12 hours. Total RNA was extracted using a RNeasy® Plus Mini Kit (Qiagen), and total
552 RNA quantified using the 2100 Bioanalyzer (Agilent). Samples with a RIN >8 was outsourced to
553 Novogene for library construction and sequencing (Illumina Platform (PE150)) with 20 M raw
554 reads/sample. The reads were mapped to the Homosapien genome (GRCh38) using STAR software
555 with ≥95% mapping rate. Differential expression analysis was performed using DESeq2 package in
556 R⁶⁴. Molecular and cellular function analysis and pathway enrichment was analyzed using Ingenuity
557 Pathway Analysis software (Qiagen). Duplicate samples were prepared for each condition.

558 *In vivo* RNA seq was also performed on orthotropic, luciferase-transfected AsPC-1 tumors.
559 Specifically, luciferase transfected AsPC-1 was implanted into pancreas, and after one week, mice
560 were treated with CK21 at 3 mg/kg for 3 days. Tumor tissues were then resected and RNA seq was
561 performed. Quadruplicate samples were prepared for each condition.

562 **Imaging Flow cytometry**

563 AsPC-1, Panc-1 were cultured with 50 nM CK21 for 24 hours and 48 hours. Cells were fixed
564 with 4% paraformaldehyde, and incubated overnight in cocktail of antibody (DPAI, anti-p65)
565 containing 0.1% Triton X-100. Stained cells were subjected to imaging flow cytometry (Amnis®

ImageStream[®]X Mk II) and images analyzed using IDEAS^R software. Specifically, the 'Similarity' feature in IDEAS^R indicates the spatial relationship between the p65 and nuclei. Low similarity scores exhibit a predominant cytoplasmic distribution of p65, whereas high similarity scores indicate a predominant nuclear distribution of p65.

Western blotting

AsPC-1, Panc-1, U049MAI, or U123M15-T were cultured with 50 nM CK21 for 24 hours. Cells then were collected, washed, and lysate for 10 min on ice. Protein concentration of each sample was detected following the protocol of Pierce[™] Detergent Compatible Bradford Assay. Total of 20 µg denatured protein was then loaded into each lane of NuPAGE[™] Bis-Tris Gel and run using Mini Gel Tank (Invitrogen). Gels were transferred to 0.45 µm Invitrolon[™] PVDF membrane using Mini Blot Module (Invitrogen). Membranes were blocked in 5% BSA overnight at 4°C. Membranes were then incubated overnight at 4°C with primary antibodies, including anti-DDIT4, anti-BCL2, anti-Caspase3, or anti-β-actin. Secondary goat anti-rabbit H&L IgG (HRP) was then incubated for one hour at room temperature. Finally, the chemiluminescent signal was enhanced by with SuperSignal[™] West Pico PLUS Chemiluminescent Substrate, and protein expression was detected using Azure[™] Biosystems 600.

RT-qPCR

Pre-designed primers were purchased from Integrated DNA Technologies, which included XBP1 (Hs.PT.58.1903847), GADD45B (Hs.PT.58.19897476.gs), MYC (Hs.PT.58.26770695), GUSB (Hs.PT.58v.27737538), VAMP1 (Hs.PT.58.26743095), POLR2A (Hs.PT.58.14390640), XIAP (Hs.PT.56a.23056448), DDIT4 (Hs.PT.58.38843854.g), ACTB (Hs.PT.56a.19461448.g) for human tumor organoid samples. DDIT4 (Mm.PT.58.43159110.g), GUSB (Mm.PT.39a.22214848), MYC (Mm.PT.58.13590978), GADD45B (Mm.PT.58.10699383.g), ACTB (Mm.PT.39a.22214843.g), XIAP (Mm.PT.56a.5536843), XBP1 (Mm.PT.58.30961962) for mouse pancreatic tumor cell line samples.

593 U049MAI or U123M15-T were cultured with 50 nM CK21 for 24 hours, total RNA was extracted
594 with an RNeasy[®] Plus Mini Kit (Qiagen) and quantified using Nanodrop 1000 spectrophotometer
595 (Thermo Fisher). RNA of each sample was reverse transcribed into cDNA using High capacity cDNA
596 reverse transcription kit (Applied Biosystems). RT-qPCR were run on QuantStudio 3 (Applied
597 Biosystems) using PowerUp[™] SYBR[™] green master mix with specific primers. RT-qPCR of murine
598 pancreatic cancer cell lines, KC-6141 and KPC-961, were prepared in the same way.

600 **Statistical analysis**

601 Data are presented as means \pm standard error (SEM). Statistical analyses were performed
602 using GraphPad Prism software. Differences between groups were analyzed using unpaired t-tests,
603 one-way or two-way ANOVA with post-hoc tests, as indicated in the figure legends.

Declaration of Interests

PZ and BQ were employees of Cinkate Pharmaceutical Corp. PZ and FX (CEO of Cinkate Pharmaceutical Corp) are listed as inventors on Patent WO2018/019301A1, which covers the design and use of CK21 for pancreatic cancer. ASC received consulting fees from Cinkate Pharmaceutical Corp. No conflicts of interest, financial or otherwise, are declared by the other authors.

Acknowledgements

This research was supported in part by a research grant (to University of Chicago) from the Cinkate Pharmaceutical Corp. We thank the Organoid and Primary Culture Research Core at University of Chicago for the gift of patient-derived pancreatic tumor organoids, the Human Tissue Resource at University of Chicago for tissue processing and staining, the Cytometry and Antibody Technology Core for advising on flow cytometry and the Animal Resources Center at University of Chicago for mouse husbandry services. Dr. Surinder K. Bartra (University of Nebraska Medical Center) provided the mouse pancreatic tumor cell lines. Dr. Barbara Bailey and Dr. Helmut Hanenberg contributed to the generation of the luciferase transfected AsPc-1. We also gratefully acknowledge Dr. Mary Buschman and Ms. Kori Kirby for advising on organoid culture, Stephanie Shen for advising on Western blotting, and Karin Peterson for training on mouse handling.

Data sharing statement

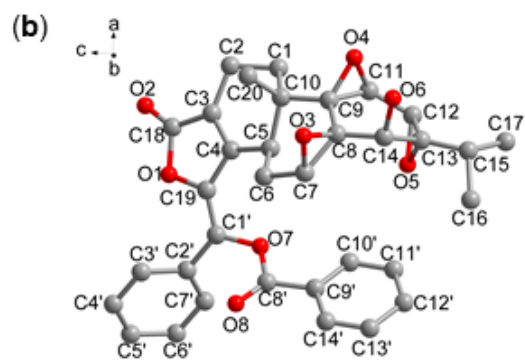
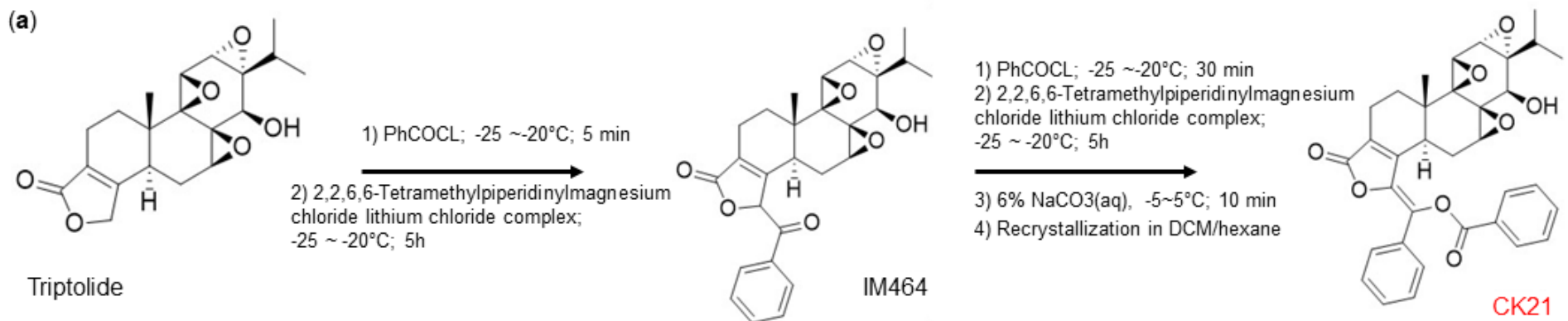
All data associated with this study are in the article or the Supplementary Materials. RNA-seq are deposited in NCBI GEO under GSE225011.

References

- 627 1. Siegel RL, Miller KD, Jemal A. Cancer statistics, 2019. *CA: A Cancer Journal for Clinicians* 2019;
628 **69**(1): 7-34.
- 629 2. Kamisawa T, Wood LD, Itoi T, Takaori K. Pancreatic cancer. *The Lancet* 2016; **388**(10039): 73-85.
- 630 3. Yachida S, Jones S, Bozic I, et al. Distant metastasis occurs late during the genetic evolution of
631 pancreatic cancer. *Nature* 2010; **467**(7319): 1114-7.
- 632 4. Sohn TA, Yeo CJ, Cameron JL, et al. Resected adenocarcinoma of the pancreas-616 patients: results,
633 outcomes, and prognostic indicators. *J Gastrointest Surg* 2000; **4**(6): 567-79.
- 634 5. Bilimoria KY, Bentrem DJ, Ko CY, Stewart AK, Winchester DP, Talamonti MS. National Failure to
635 Operate on Early Stage Pancreatic Cancer. *Annals of Surgery* 2007; **246**(2): 173-80.
- 636 6. Oettle H, Neuhaus P, Hochhaus A, et al. Adjuvant Chemotherapy With Gemcitabine and Long-term
637 Outcomes Among Patients With Resected Pancreatic Cancer. *JAMA* 2013; **310**(14): 1473.
- 638 7. Burris HA, 3rd, Moore MJ, Andersen J, et al. Improvements in survival and clinical benefit with
639 gemcitabine as first-line therapy for patients with advanced pancreas cancer: a randomized trial. *J Clin Oncol*
640 1997; **15**(6): 2403-13.
- 641 8. Von Hoff DD, Ervin T, Arena FP, et al. Increased survival in pancreatic cancer with nab-paclitaxel plus
642 gemcitabine. *N Engl J Med* 2013; **369**(18): 1691-703.
- 643 9. Conroy T, Desseigne F, Ychou M, et al. FOLFIRINOX versus gemcitabine for metastatic pancreatic
644 cancer. *N Engl J Med* 2011; **364**(19): 1817-25.
- 645 10. Kupchan SM, Court WA, Dailey RG, Gilmore CJ, Bryan RF. Tumor inhibitors. LXXIV. Triptolide and
646 triptidiolide, novel antileukemic diterpenoid triepoxides from *Tripterygium wilfordii*. *Journal of the American*
647 *Chemical Society* 1972; **94**(20): 7194-5.
- 648 11. He J, Peng T, Peng Y, et al. Molecularly Engineering Triptolide with Aptamers for High Specificity and
649 Cytotoxicity for Triple-Negative Breast Cancer. *Journal of the American Chemical Society* 2020; **142**(6): 2699-
650 703.
- 651 12. Li J, Liu R, Yang Y, et al. Triptolide-induced in vitro and in vivo cytotoxicity in human breast cancer
652 stem cells and primary breast cancer cells. *Oncology Reports* 2014; **31**(5): 2181-6.
- 653 13. Liu Q. Triptolide and its expanding multiple pharmacological functions. *International*
654 *Immunopharmacology* 2011; **11**(3): 377-83.
- 655 14. Jiang C, Fang X, Zhang H, et al. Triptolide inhibits the growth of osteosarcoma by regulating
656 microRNA-181a via targeting PTEN gene in vivo and vitro. *Tumor Biology* 2017; **39**(4): 101042831769755.
- 657 15. Reno TA, Kim JY, Raz DJ. Triptolide Inhibits Lung Cancer Cell Migration, Invasion, and Metastasis.
658 *The Annals of Thoracic Surgery* 2015; **100**(5): 1817-25.
- 659 16. Song JM, Molla K, Anandharaj A, et al. Triptolide suppresses the in vitro and in vivo growth of lung
660 cancer cells by targeting hyaluronan-CD44/RHAMM signaling. *Oncotarget* 2017; **8**(16): 26927-40.
- 661 17. Carter BZ, Mak DH, Shi Y, et al. MRx102, a triptolide derivative, has potent antileukemic activity in
662 vitro and in a murine model of AML. *Leukemia* 2012; **26**(3): 443-50.
- 663 18. Carter BZ, Mak DH, Schober WD, et al. Triptolide induces caspase-dependent cell death mediated via
664 the mitochondrial pathway in leukemic cells. *Blood* 2006; **108**(2): 630-7.
- 665 19. Hu H, Luo L, Liu F, et al. Anti-cancer and Sensibilisation Effect of Triptolide on Human Epithelial
666 Ovarian Cancer. *Journal of Cancer* 2016; **7**(14): 2093-9.
- 667 20. Zhao H, Yang Z, Wang X, et al. Triptolide inhibits ovarian cancer cell invasion by repression of matrix
668 metalloproteinase 7 and 19 and upregulation of E-cadherin. *Experimental & Molecular Medicine* 2012; **44**(11):
669 633.
- 670 21. Huang W, He T, Chai C, et al. Triptolide Inhibits the Proliferation of Prostate Cancer Cells and Down-
671 Regulates SUMO-Specific Protease 1 Expression. *PLoS ONE* 2012; **7**(5): e37693.
- 672 22. Yang S, Chen J, Guo Z, et al. Triptolide inhibits the growth and metastasis of solid tumors. *Mol Cancer*
673 *Ther* 2003; **2**(1): 65-72.

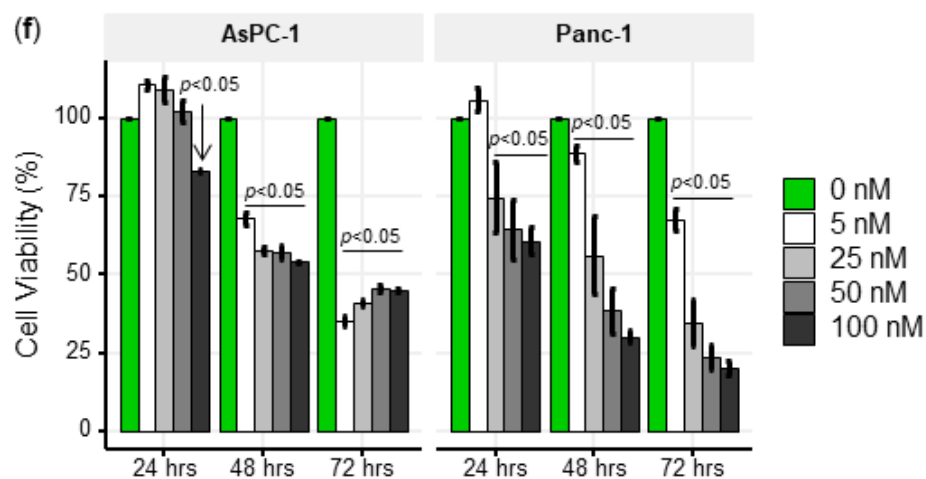
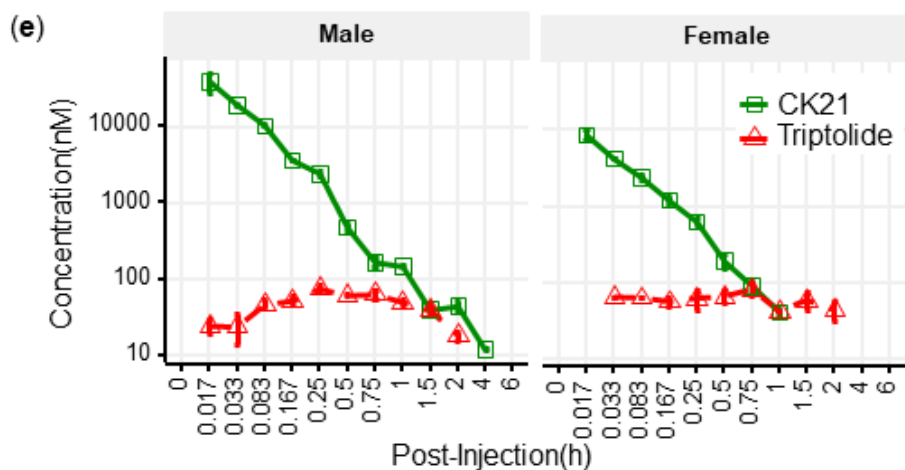
- 674 23. Wang Z, Jin H, Xu R, Mei Q, Fan D. Triptolide downregulates Rac1 and the JAK/STAT3 pathway and
675 inhibits colitis-related colon cancer progression. *Experimental and Molecular Medicine* 2009; **41**(10): 717.
- 676 24. Chugh R, Sangwan V, Patil SP, et al. A Preclinical Evaluation of Minnelide as a Therapeutic Agent
677 Against Pancreatic Cancer. *Science Translational Medicine* 2012; **4**(156): 156ra39-ra1.
- 678 25. Wang W, Li X, Sun W, et al. Triptolide triggers the apoptosis of pancreatic cancer cells via the
679 downregulation of Decoy receptor 3 expression. *Journal of Cancer Research and Clinical Oncology* 2012;
680 **138**(9): 1597-605.
- 681 26. Lee KY, Park JS, Jee YK, Rosen GD. Triptolide sensitizes lung cancer cells to TNF-related apoptosis-
682 inducing ligand (TRAIL)-induced apoptosis by inhibition of NF-kappaB activation. *Exp Mol Med* 2002; **34**(6):
683 462-8.
- 684 27. Phillips PA, Dudeja V, McCarroll JA, et al. Triptolide Induces Pancreatic Cancer Cell Death via
685 Inhibition of Heat Shock Protein 70. *Cancer Research* 2007; **67**(19): 9407-16.
- 686 28. Titov DV, Gilman B, He Q-L, et al. XPB, a subunit of TFIIH, is a target of the natural product triptolide.
687 *Nature Chemical Biology* 2011; **7**(3): 182-8.
- 688 29. Noel P, Von Hoff DD, Saluja AK, Velagapudi M, Borazanci E, Han H. Triptolide and Its Derivatives as
689 Cancer Therapies. *Trends in Pharmacological Sciences* 2019; **40**(5): 327-41.
- 690 30. Tong L, Zhao Q, Datan E, et al. Triptolide: reflections on two decades of research and prospects for the
691 future. *Nat Prod Rep* 2021; **38**(4): 843-60.
- 692 31. Kitzen JJEM, De Jonge MJA, Lamers CHJ, et al. Phase I dose-escalation study of F60008, a novel
693 apoptosis inducer, in patients with advanced solid tumours. *European Journal of Cancer* 2009; **45**(10): 1764-
694 72.
- 695 32. Greeno E, Borazanci E, Gockerman J, Korn R, Saluja A, Von Hoff D. Abstract CT207: Phase I dose
696 escalation and pharmacokinetic study of 14-O-phosphonoxyethyltriptolide. *Cancer Research* 2015; **75**(15
697 Supplement): CT207.
- 698 33. Qiu W, Su GH. Challenges and advances in mouse modeling for human pancreatic tumorigenesis and
699 metastasis. *Cancer Metastasis Rev* 2013; **32**(1-2): 83-107.
- 700 34. Shannon HE, Fishel ML, Xie J, et al. Longitudinal Bioluminescence Imaging of Primary Versus
701 Abdominal Metastatic Tumor Growth in Orthotopic Pancreatic Tumor Models in NSG Mice. *Pancreas* 2015;
702 **44**(1): 64-75.
- 703 35. Weeber F, Ooft SN, Dijkstra KK, Voest EE. Tumor Organoids as a Pre-clinical Cancer Model for Drug
704 Discovery. *Cell Chemical Biology* 2017; **24**(9): 1092-100.
- 705 36. Huang L, Holtzinger A, Jagan I, et al. Ductal pancreatic cancer modeling and drug screening using
706 human pluripotent stem cell- and patient-derived tumor organoids. *Nat Med* 2015; **21**(11): 1364-71.
- 707 37. Seino T, Kawasaki S, Shimokawa M, et al. Human Pancreatic Tumor Organoids Reveal Loss of Stem
708 Cell Niche Factor Dependence during Disease Progression. *Cell Stem Cell* 2018; **22**(3): 454-67 e6.
- 709 38. Boj SF, Hwang CI, Baker LA, et al. Organoid models of human and mouse ductal pancreatic cancer.
710 *Cell* 2015; **160**(1-2): 324-38.
- 711 39. Romero-Calvo I, Weber CR, Ray M, et al. Human Organoids Share Structural and Genetic Features
712 with Primary Pancreatic Adenocarcinoma Tumors. *Molecular Cancer Research* 2019; **17**(1): 70-83.
- 713 40. Pinto JA, Rolfo C, Raez LE, et al. In silico evaluation of DNA Damage Inducible Transcript 4 gene
714 (DDIT4) as prognostic biomarker in several malignancies. *Scientific Reports* 2017; **7**(1).
- 715 41. Park M, Hong J. Roles of NF-κB in Cancer and Inflammatory Diseases and Their Therapeutic
716 Approaches. *Cells* 2016; **5**(2): 15.
- 717 42. Liptay S, Weber CK, Ludwig L, Wagner M, Adler G, Schmid RM. Mitogenic and antiapoptotic role of
718 constitutive NF-kappaB/Rel activity in pancreatic cancer. *Int J Cancer* 2003; **105**(6): 735-46.
- 719 43. Dolcet X, Llobet D, Pallares J, Matias-Guiu X. NF-kB in development and progression of human
720 cancer. *Virchows Arch* 2005; **446**(5): 475-82.
- 721 44. Marquez-Jurado S, Diaz-Colunga J, das Neves RP, et al. Mitochondrial levels determine variability in
722 cell death by modulating apoptotic gene expression. *Nat Commun* 2018; **9**(1): 389.

- 723 45. Redza-Dutordoir M, Averill-Bates DA. Activation of apoptosis signalling pathways by reactive oxygen
724 species. *Biochim Biophys Acta* 2016; **1863**(12): 2977-92.
- 725 46. Chen BJ. Triptolide, A Novel Immunosuppressive and Anti-Inflammatory Agent Purified from a
726 Chinese Herb *Tripterygium Wilfordii* Hook F. 2001; **42**(3): 253-65.
- 727 47. Torres MP, Rachagani S, Soucek JJ, Mallya K, Johansson SL, Batra SK. Novel Pancreatic Cancer Cell
728 Lines Derived from Genetically Engineered Mouse Models of Spontaneous Pancreatic Adenocarcinoma:
729 Applications in Diagnosis and Therapy. *PLoS ONE* 2013; **8**(11): e80580.
- 730 48. Li XJ, Jiang ZZ, Zhang LY. Triptolide: progress on research in pharmacodynamics and toxicology. *J*
731 *Ethnopharmacol* 2014; **155**(1): 67-79.
- 732 49. Liu L, Jiang Z, Liu J, et al. Sex differences in subacute toxicity and hepatic microsomal metabolism of
733 triptolide in rats. *Toxicology* 2010; **271**(1-2): 57-63.
- 734 50. Xue X, Gong L, Qi X, et al. Knockout of hepatic P450 reductase aggravates triptolide-induced toxicity.
735 *Toxicol Lett* 2011; **205**(1): 47-54.
- 736 51. Fidler JM, An J, Carter BZ, Andreeff M. Preclinical antileukemic activity, toxicology, toxicokinetics
737 and formulation development of triptolide derivative MRx102. *Cancer Chemother Pharmacol* 2014; **73**(5):
738 961-74.
- 739 52. Chen F, Gao X, Shilatifard A. Stably paused genes revealed through inhibition of transcription initiation
740 by the TFIID inhibitor triptolide. *Genes & Development* 2015; **29**(1): 39-47.
- 741 53. Santo L, Vallet S, Hideshima T, et al. AT7519, A novel small molecule multi-cyclin-dependent kinase
742 inhibitor, induces apoptosis in multiple myeloma via GSK-3beta activation and RNA polymerase II inhibition.
743 *Oncogene* 2010; **29**(16): 2325-36.
- 744 54. Cai D, Latham VM, Jr., Zhang X, Shapiro GI. Correction: Combined Depletion of Cell Cycle and
745 Transcriptional Cyclin-Dependent Kinase Activities Induces Apoptosis in Cancer Cells. *Cancer Res* 2020;
746 **80**(2): 361.
- 747 55. Albensi BC. What Is Nuclear Factor Kappa B (NF-kappa B) Doing in and to the Mitochondrion?
748 *Frontiers in Cell and Developmental Biology* 2019; **7**.
- 749 56. Pazarentzos E, Mahul-Mellier AL, Datler C, et al. I kappa B alpha inhibits apoptosis at the outer
750 mitochondrial membrane independently of NF-kappa B retention. *Embo Journal* 2014; **33**(23): 2814-28.
- 751 57. Liu H, Ma Y, Pagliari LJ, et al. TNF-alpha-induced apoptosis of macrophages following inhibition of
752 NF-kappa B: a central role for disruption of mitochondria. *J Immunol* 2004; **172**(3): 1907-15.
- 753 58. Adams JM, Cory S. Life-or-death decisions by the Bcl-2 protein family. *Trends Biochem Sci* 2001;
754 **26**(1): 61-6.
- 755 59. Vaux DL, Cory S, Adams JM. Bcl-2 gene promotes haemopoietic cell survival and cooperates with c-
756 myc to immortalize pre-B cells. *Nature* 1988; **335**(6189): 440-2.
- 757 60. Wolter KG, Hsu YT, Smith CL, Nechushtan A, Xi XG, Youle RJ. Movement of Bax from the cytosol to
758 mitochondria during apoptosis. *J Cell Biol* 1997; **139**(5): 1281-92.
- 759 61. Ly JD, Grubb DR, Lawen A. The mitochondrial membrane potential (deltapsi(m)) in apoptosis; an
760 update. *Apoptosis* 2003; **8**(2): 115-28.
- 761 62. Gross A, McDonnell JM, Korsmeyer SJ. BCL-2 family members and the mitochondria in apoptosis.
762 *Genes Dev* 1999; **13**(15): 1899-911.
- 763 63. Tao Y, Zhang ML, Ma PC, et al. Triptolide inhibits proliferation and induces apoptosis of human
764 melanoma A375 cells. *Asian Pac J Cancer Prev* 2012; **13**(4): 1611-5.
- 765 64. Anders S, Huber W. Differential expression analysis for sequence count data. *Genome Biology* 2010;
766 **11**(10): R106.
- 767
- 768

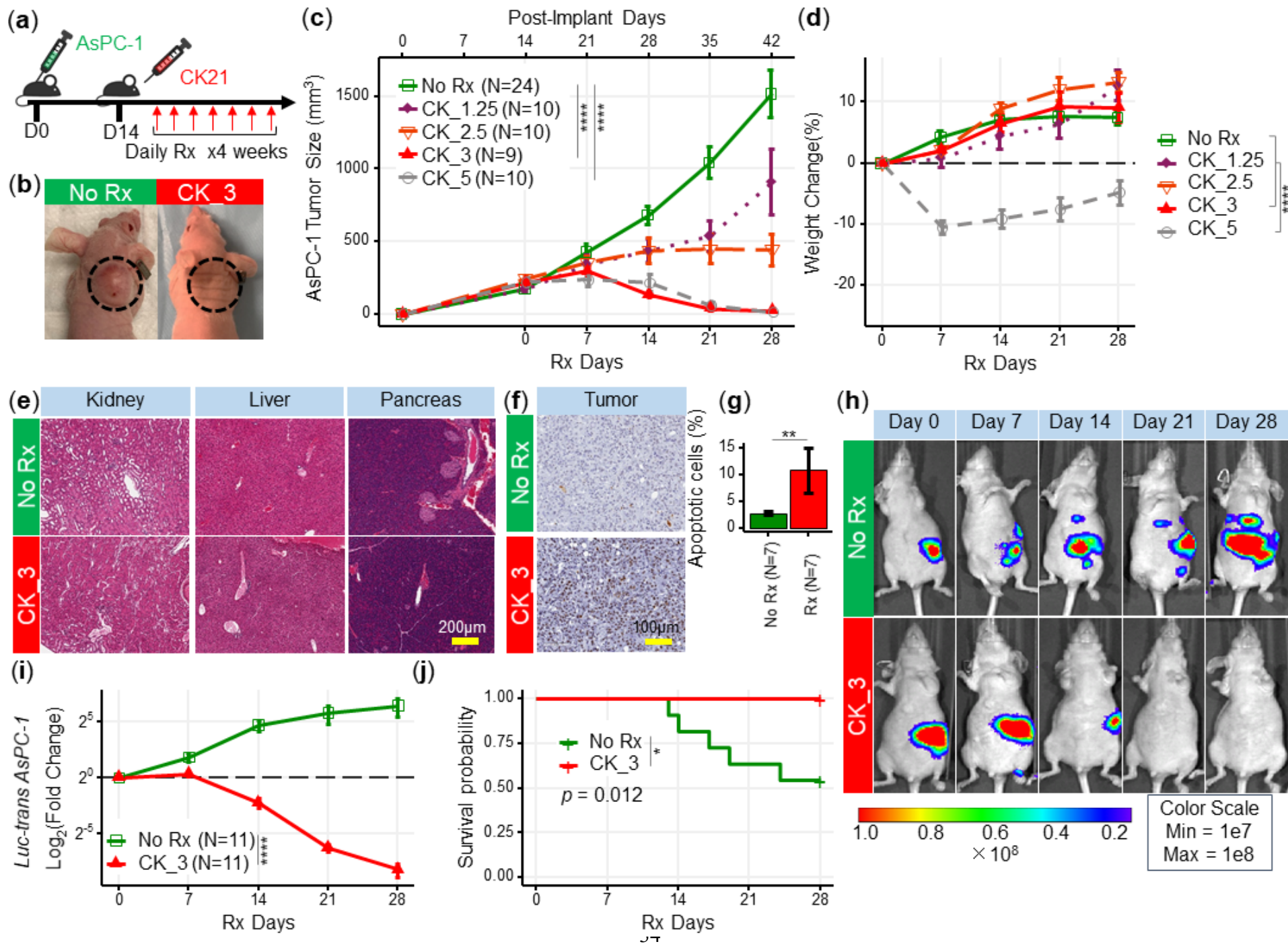


(c)

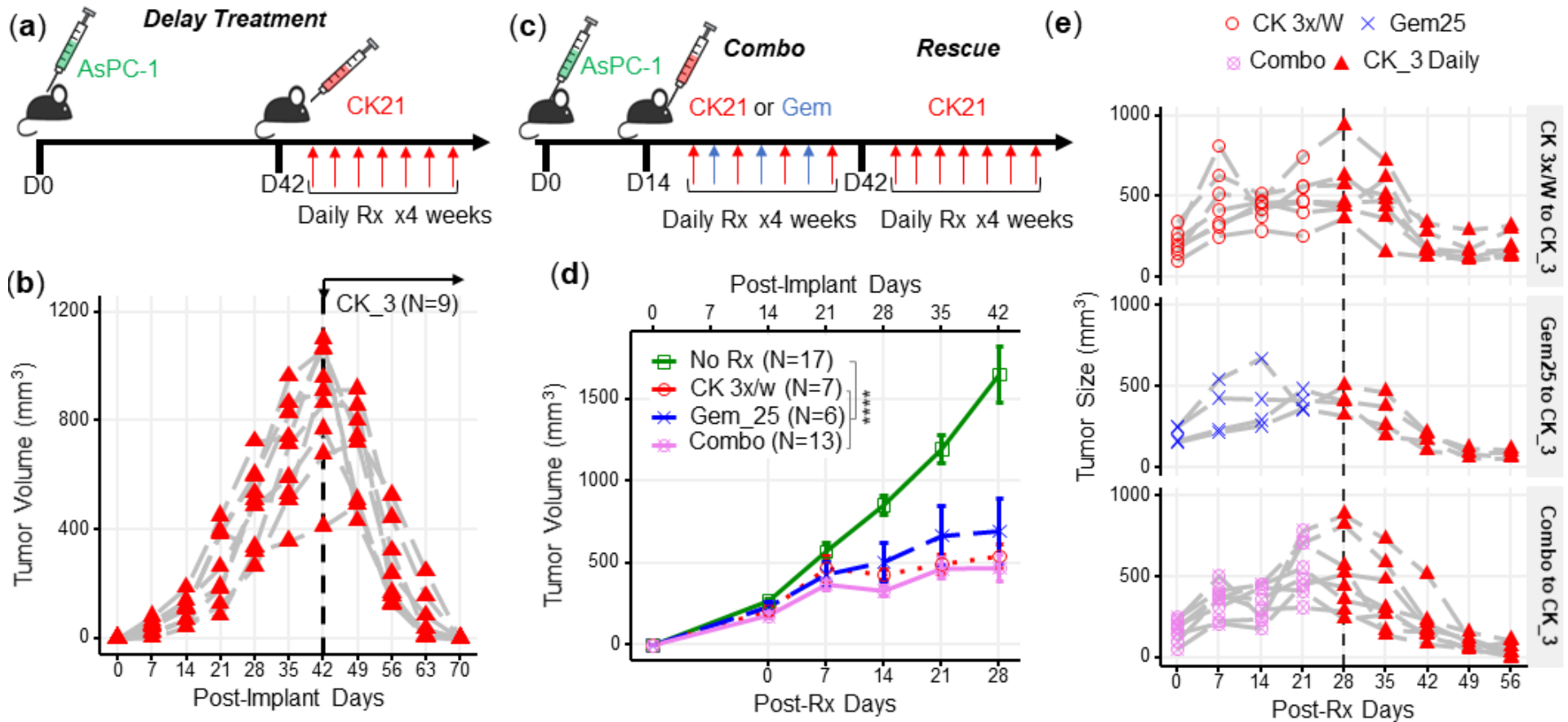
Components	Function	Content (%)
CK21	API	0.03
Medium chain triglycerides	Oil phase	20
Phospholipids	Emulsifier	2
Glycerol	Isotonic moderator	2.25
DSPE-MPEG2000	Co-emulsifier	0.3
Water for injection	Water phase	77



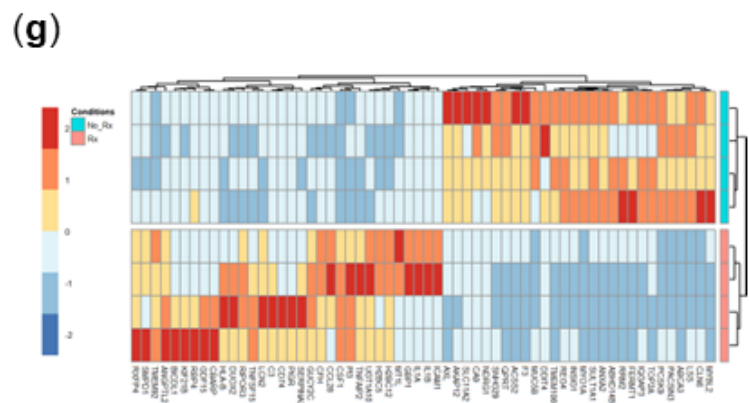
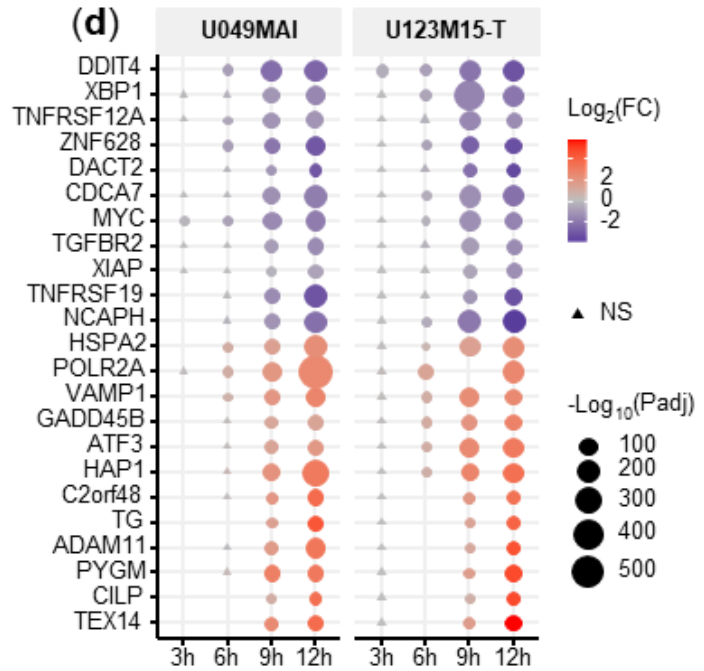
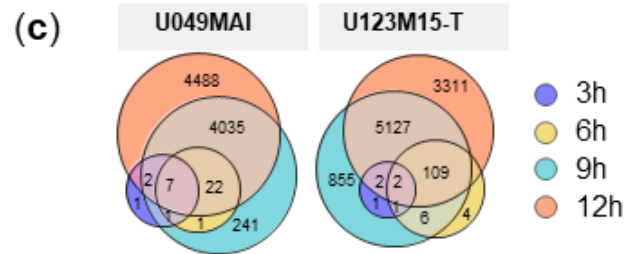
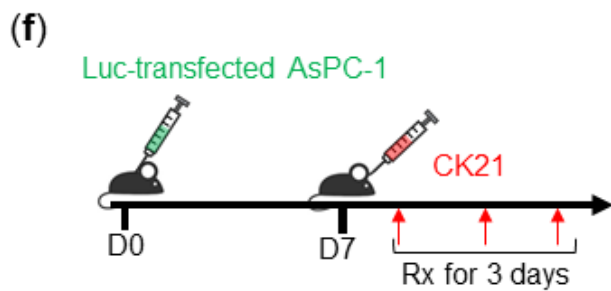
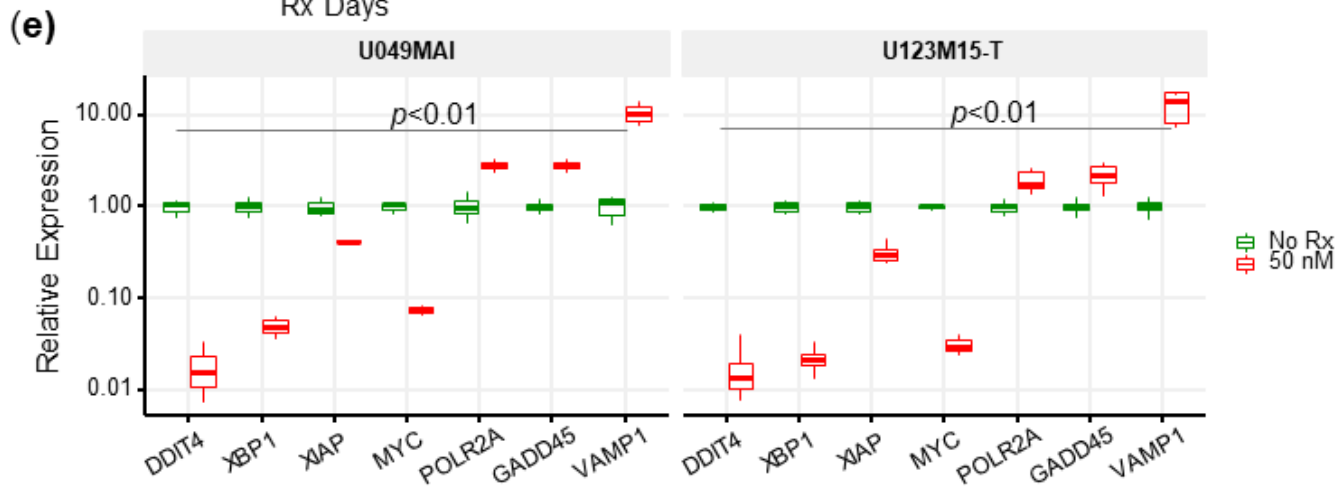
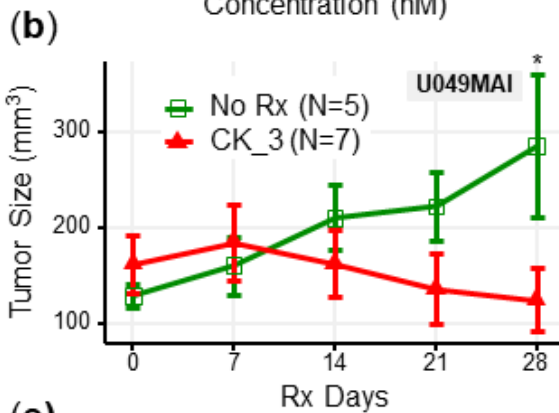
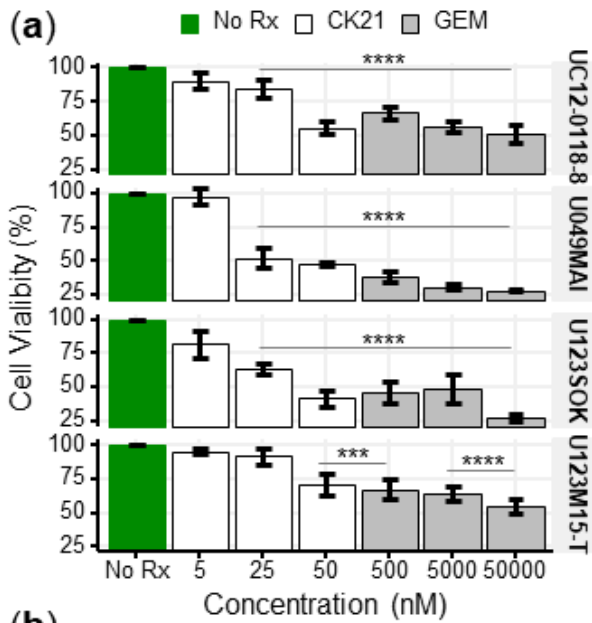
771 **Fig.1. CK21 exhibits a stable release of triptolide *in vivo*.** (a) Synthesis of compound CK21 as white solid after recrystallization in a mixed
772 organic solvent. Compound structure was characterized by H-NMR, C-NMR and HR-MS. (b) Thermal ellipsoid model illustrating the crystal
773 structure of CK21; carbon atoms were shown in gray, and oxygen atoms in red. Hydrogen atoms were omitted for clarity (c) Composition and
774 putative function in the CK21 fat emulsion. (d) Macroscopic image of the final emulsion product of CK21. (e) *In vivo* administration of CK21 into SD
775 rats (3 rats per group) converted into triptolide. CK21 was injected intravenously into female (1.5 mg/kg) and male (3 mg/kg) rats, and the
776 concentration of CK21 and triptolide in the plasma was quantified. For samples ≥ 4 hours, no CK21 or triptolide was detected. (f) CK21 inhibited
777 the proliferation of human pancreatic cancer cell lines. Data presented in all the graphs are mean \pm standard error. Statistical analysis: Two-way
778 ANOVA (repeated measures) with post-hoc comparison of the means was conducted for (f).



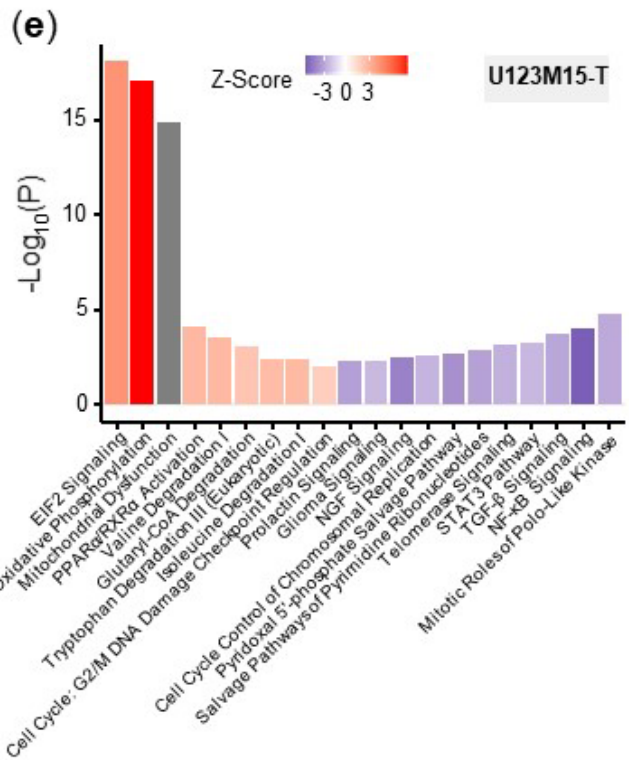
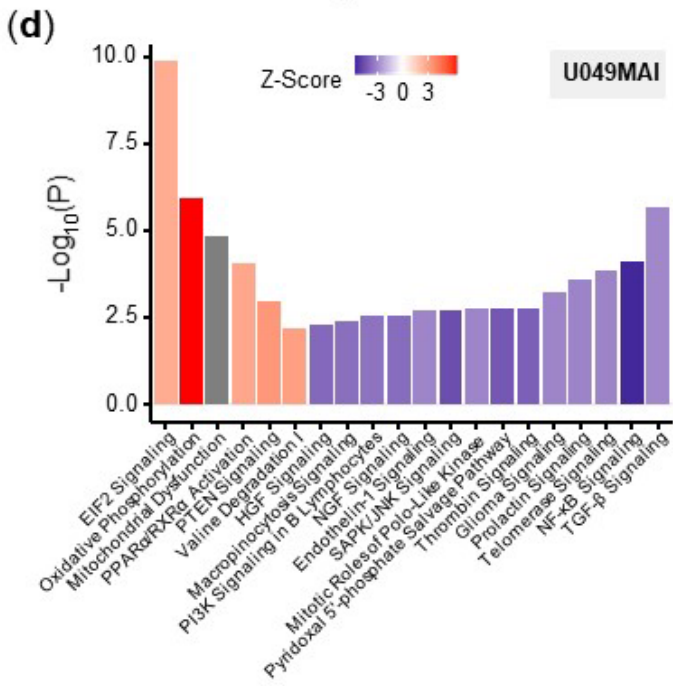
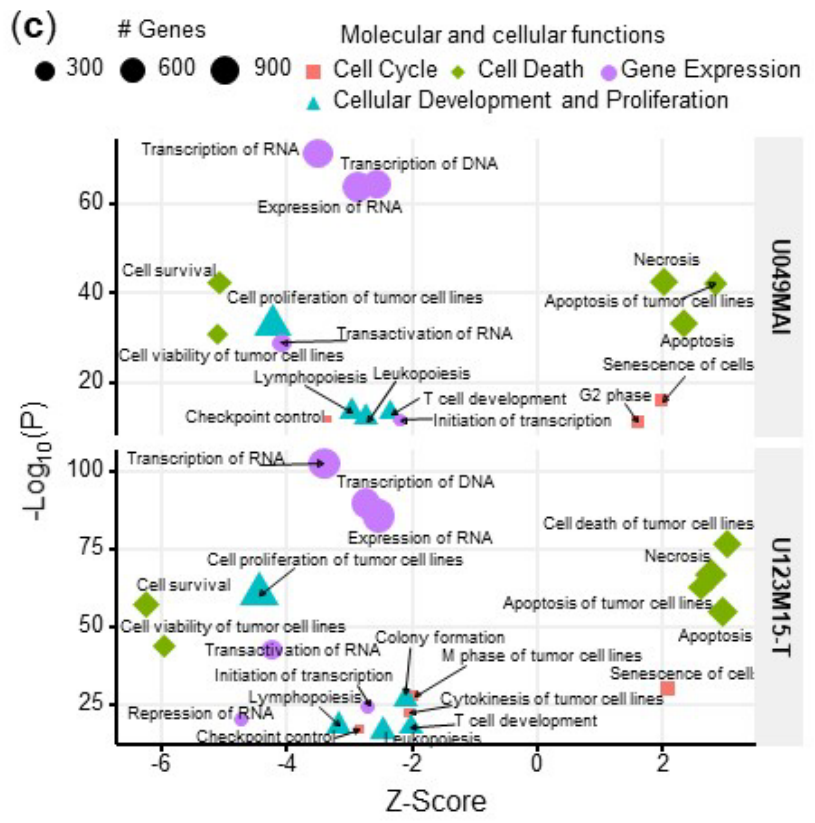
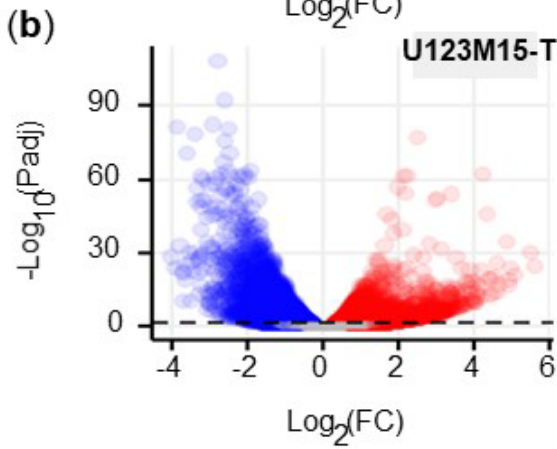
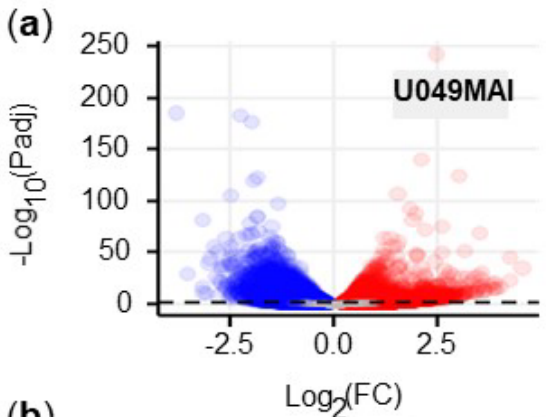
780 **Fig.2. CK21 shows efficacy and minimal toxicity at 3 mg/kg in different *in vivo* animal models.** (a) Scheme of *in vivo* efficacy studies. Human
781 pancreatic cancer cell line, AsPc-1, was implanted into nude mice and CK21 treatment was initiated ~14 days later and administered daily for 4
782 weeks. (b) Macroscopic images of tumor-bearing nude mice after receiving CK21 or blank emulsion after 4 weeks treatment. (c) AsPC-1 tumor
783 volume after subcutaneous implantation and CK21 or gemcitabine treatment. (d) Weight change of the nude mice bearing AsPC-1 and receiving
784 CK21. (e) H&E staining of mice organ tissues after CK21 treatment. (f) TUNEL staining of tumor tissue and (g) percentage of apoptotic cells in
785 AsPC-1 tumor after 2 weeks CK21. (h) Bioluminescence images of nude mice bearing intra-pancreatic AsPC-1 and receiving CK21. Color scheme
786 represents the intensity of luminescence reflecting tumor size in each mouse. Mice with higher initial tumor burden was placed into Rx group, and
787 those with lower initial tumor burden into control group. (i) Fold change of the luminescence intensity of the nude mice bearing intra-pancreatic
788 AsPC-1. (j) Survival curve of mice with orthotopic AsPC-1 tumors receiving CK21 treatment. In all the figures, post-implant days are days after
789 tumor implantation and post-Rx days are days after receiving CK21 treatment (doses indicated as mg/kg). Data presented in all the graphs are
790 mean \pm standard error (some error bars are too small to be visible). Statistical analysis: Two-way ANOVA (not repeated measures) with post-hoc
791 comparison of the means of each data set was conducted for all the line graphs except (i); For survival curve, Log-rank (Mantel-Cox) test was
792 applied. (* $p < 0.05$, ** $p < 0.01$, *** $p < 0.001$, **** $p < 0.0001$)



793
 794 **Fig.3. CK21 of 3 mg/kg daily shows efficacy in delay therapy and rescues mice that failed in synergistic therapy.** (a) Scheme of delayed
 795 therapy. Mice received CK21 at 3 mg/kg daily for 4 weeks, starting on day 42 post-tumor inoculation. (b) Tumor volume during delayed CK21
 796 therapy. (c) Scheme of synergistic and rescue therapy. Mice receive CK21 3 mg/kg (3X/week; Mo, We, Fr), gemcitabine at 25 mg/kg (3X/week; Tu,
 797 Th, Sa), or both. (d) Tumor size during the synergistic therapy of CK21. (e) Mice which failed at CK21 or gemcitabine or synergistic therapy from
 798 (c-d) were then rescued by switching to CK21 at 3 mg/kg daily, and tumor size monitored. Post-implant days are days after tumor implantation.
 799 Post-Rx days are days after receiving CK21 treatment. Data presented in (d) are mean \pm standard error. Statistical analysis: Two-way ANOVA (not
 800 repeated measures) with post-hoc comparison of the means of each data set was conducted for (d), (**** $p < 0.0001$). Each line in (b) and (e)
 801 represents a single mouse.

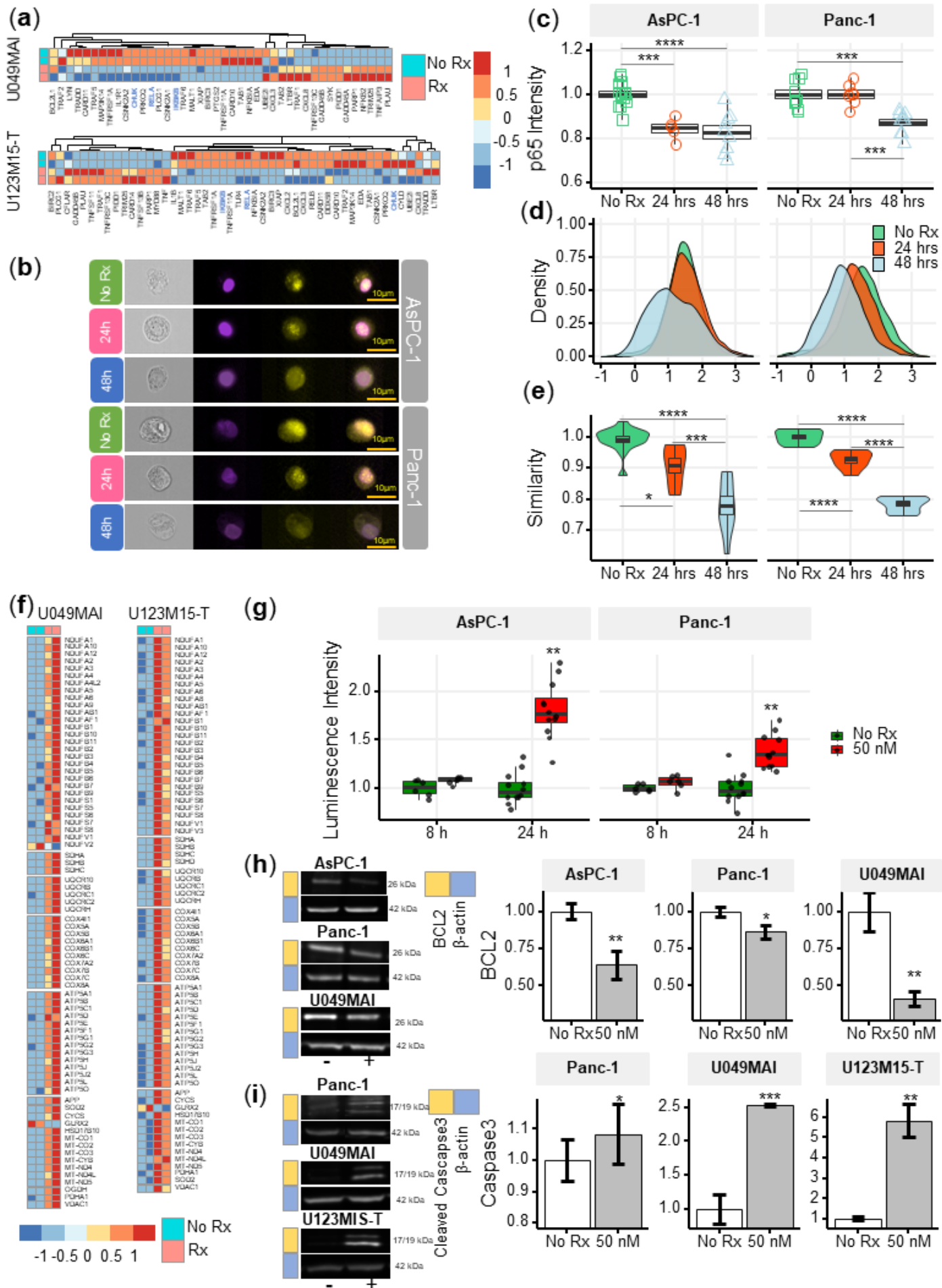


803 **Fig.4. Transcriptome analysis of patient-derived pancreatic tumor organoids after CK21 treatment. (a)**
804 *In vitro* culture of different organoids with escalating concentrations of CK21 for 72h. Gemcitabine was included
805 as a positive control. **(b)** U049MAI tumor size in nude mice during CK21 treatment. **(c)** Co-expression Venn
806 diagram of differentially expressed genes that were significantly different with CK21 treatment. Size of the
807 circles reflect the total number of differentially expressed genes (transformed using $\log_2(n+1)$). **(d)** Genes of
808 interest showing consistent up or down regulation as treatment time increased. Fold change is color coded
809 where red is upregulation, blue is down regulation. Circle presents the genes had an adjusted p value < 0.05,
810 and triangle presents the genes had an adjusted p value > 0.05. Size of the circle represents the adjusted p
811 values. **(e)** RT-qPCR analysis of gene expression in tumor organoids after CK21 treatment for 24h. **(f)** Scheme
812 of RNA seq using *in vivo* orthotopic AsPC-1 model. **(g)** Heatmaps of top statistically significant differentially
813 expressed genes in AsPC-1 tumors after treatment with CK21 for three days. Statistical analysis: Two-way
814 ANOVA (not repeated measures) with post-hoc comparison of the means of each drug dose was compared to
815 No Rx controls for **(a)**. Line indicates the doses that resulted in significant reduction in viability by CK21 or
816 gemcitabine. Two-way ANOVA with post-hoc comparison of the means of each time point was conducted for
817 **(b)**, Multiple t tests were conducted for **(e)** (** $p < 0.01$, *** $p < 0.001$, **** $p < 0.0001$)
818
819



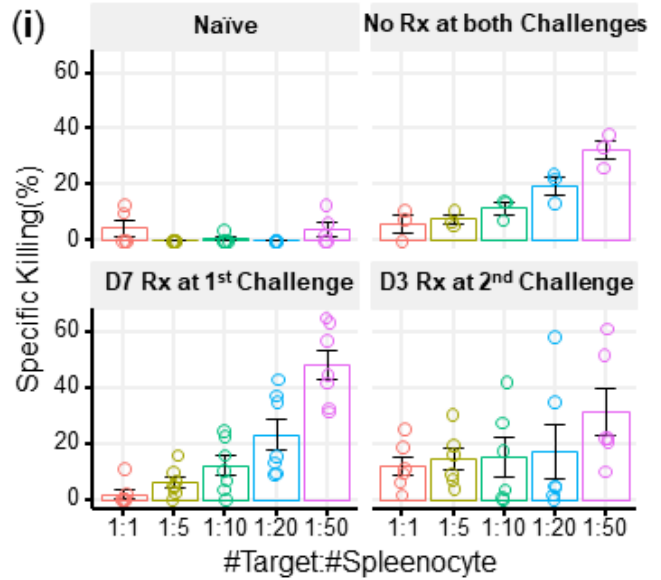
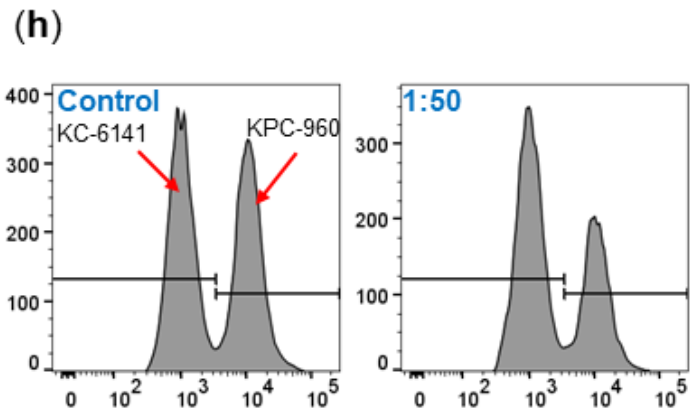
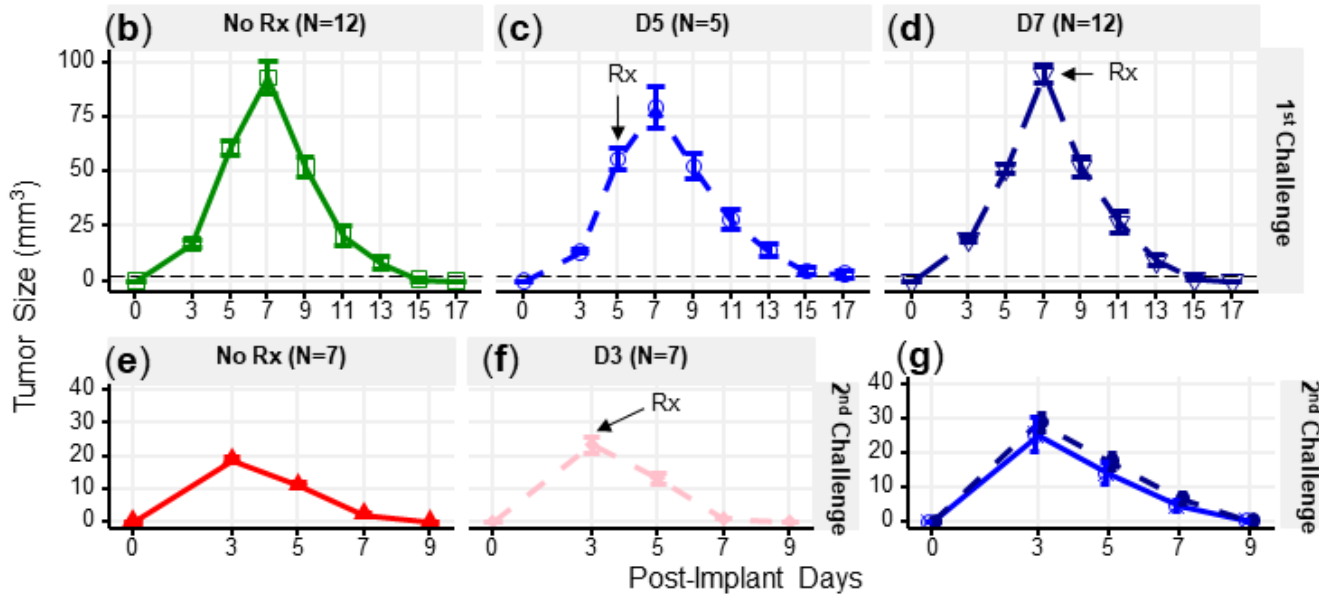
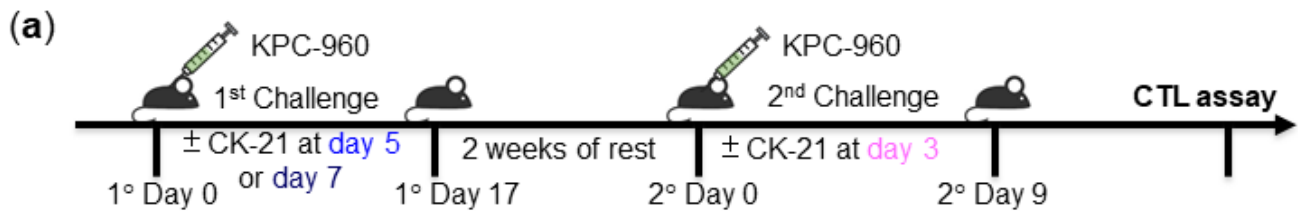
820
821
822
823

824 **Fig.5. Bioinformatic analysis of the effect of CK21 on patient-derived pancreatic tumor organoids. (a)**
825 Volcano plots of differentially expressed genes in (a) U049MAI and (b) U123M15-T after 12 h CK21 treatment
826 (50 nM). Significance cutoff was $p < 0.05$. Upregulation was colored as red, and downregulation was colored
827 as blue. (c) Enrichment of molecular and cellular functions in U049MAI and U123M15-T after CK21 treatment.
828 Size represents gene numbers. Color and shape represent functional groups. Z-score represents the
829 confidence of the prediction, where positive value means upregulation and negative value means
830 downregulation. Canonical pathway enrichment in (d) U049MAI and (e) U123M15-T after treatment with CK21
831 at 50 nM. Color represent Z-score where red means upregulation and blue means downregulation. Statistical
832 analysis: Unpaired t-test was conducted for (c); Data presented in all the bar graphs are mean \pm standard
833 error.



835
836
837
838
839
840
841
842
843
844
845
846
847

Fig.6. CK21 inhibits NF- κ B activation and induces mitochondrial mediated apoptosis. (a) Heatmap of the relative expression of genes in the NF- κ B pathway in U049MAI and U123M15-T after CK21 treatment. Genes are color coded where red means upregulated, and blue means downregulated. Only statistically significant genes are listed. (b) Representative p65 translocation images of AsPC-1 and Panc-1 after treated with CK21 at 50 nM. Nuclei stained as purple, p65 stained as yellow. (c) Relative p65 MFI of AsPC-1 and Panc-1 after CK21 (50 nM) treatment. (d) Density plots and (e) similarity scores of p65 for AsPC-1 and Panc-1. (f) Heatmaps of genes involved in oxidative phosphorylation of U049MAI and U123M15-T after CK21 treatment. (g) Reactive oxygen species generated after CK21 treatment (8 and 24 hours). Representative blotting images and quantification of (h) BCL2 expression and (i) cleaved caspase-3 at 24 hours after CK21 treatment. Statistical analysis: One-way ANOVA with post-hoc Tukey comparison of the means of each data set was conducted for (c), (e); Unpaired T test was conducted at different time points for (g), (h), (i). (* $p < 0.05$, ** $p < 0.01$, *** $p < 0.001$, **** $p < 0.0001$)

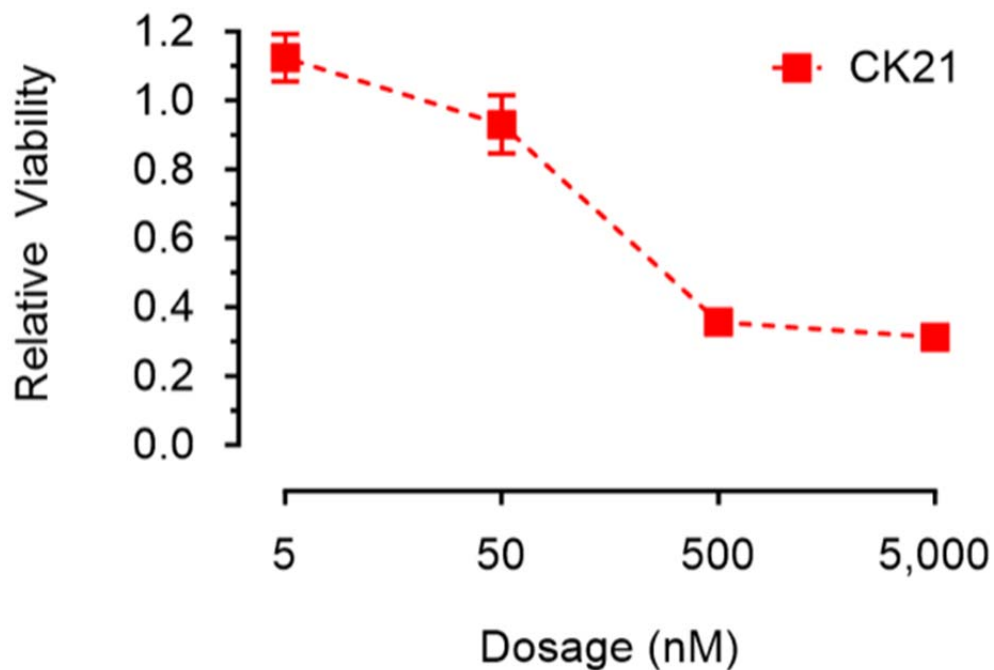


848
849
850
851
852
853
854

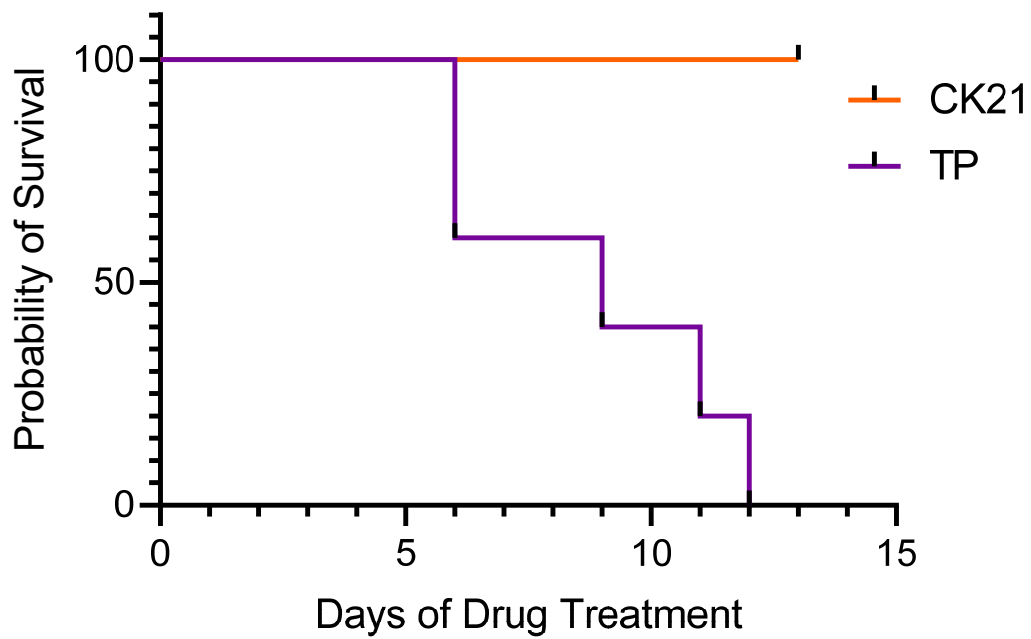
855 **Fig.7. CK21 does not exhibit significant immunosuppression in a spontaneous tumor rejection model.**

856 (a) Scheme of a subcutaneous model of mouse pancreatic tumor, KPC-960, with CK21 treatment. CK21 was
857 provided at 3 mg/kg daily starting on day 5 or day 7. During secondary challenge, CK21 was provided at 3
858 mg/kg daily from day 3 post-tumor implantation. Tumor size of mice receiving first challenge (b) without any
859 CK21, (c) with CK21 starting on day 5. (d) or day 7. Tumor size of mice receiving a second challenge (e)
860 without any CK21, or (f) with CK21 treatment starting on day 3. (g) Mice that cleared KPC-960 tumor in (c) and
861 (d) received a second tumor challenge without any CK21; tumor size were quantified weekly (h) Flow plots of
862 CTL assay, another mouse pancreatic tumor, KC-6141, was used as a non-specific target. Quantification of the
863 recovered KPC-960 compared to KC-6141, as a quantification of specific cytotoxic T cell (CTL) killing. (i)
864 Specific CTL killing of KPC-960 cells with splenocytes from (e), (f), (g). Splenocytes from naïve mice was
865 included as a negative control. Data presented in all the graphs are mean \pm standard error. Statistical analysis:
866 Two-way ANOVA with post-hoc comparison of the means of each time point was conducted for (b) and (e), (*
867 $p < 0.05$, ** $p < 0.01$, *** $p < 0.001$).
868

869 **Figure supplements**



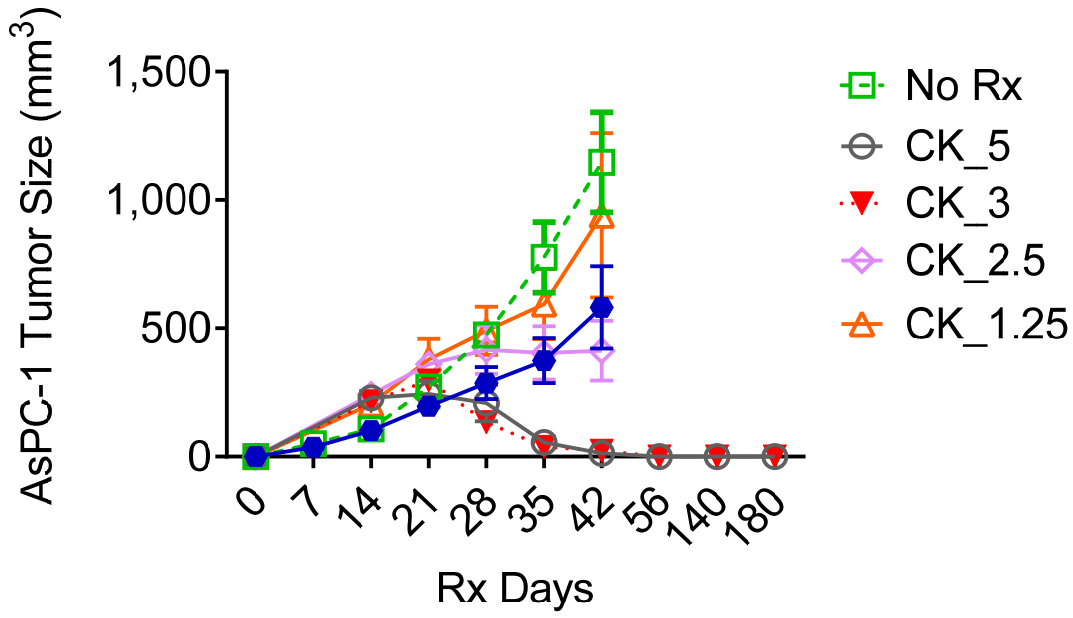
870
871 Figure 1-figure supplement 1. In vitro viability assay of primary human fibroblasts cocultured with CK21 at the
872 indicated concentrations for 72 hours.
873



874

875 Figure 2-figure supplement 1. Survival curve of mice receiving CK21 at 5mg/kg or triptolide (TP) at 0.25
876 mg/kg

877



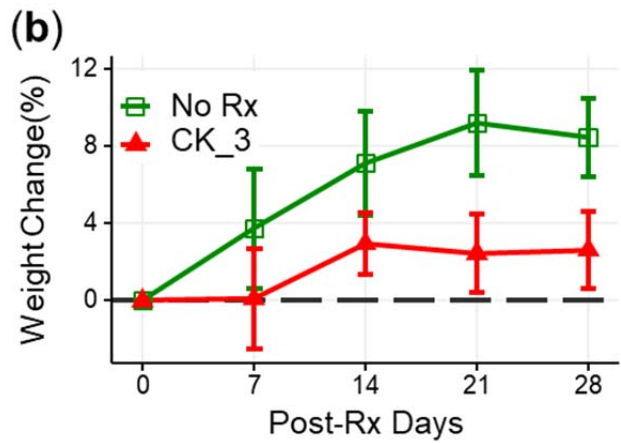
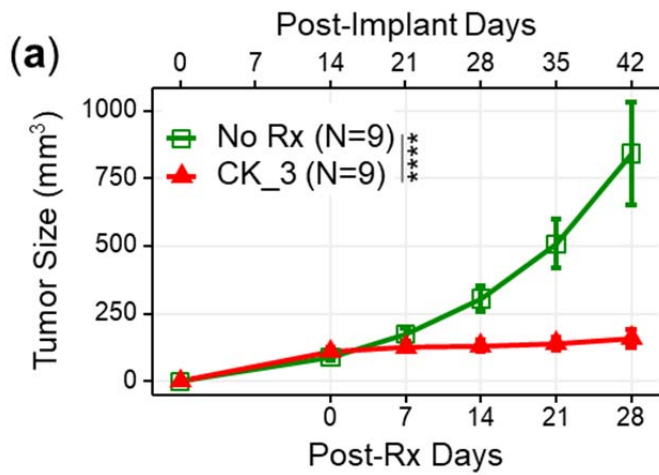
878

879

880

881

Figure 2-figure supplement 2. AsPC-1 subcutaneous tumors showed no tumor relapse after treated with CK21 at 5 or 3 mg/kg.



882

883

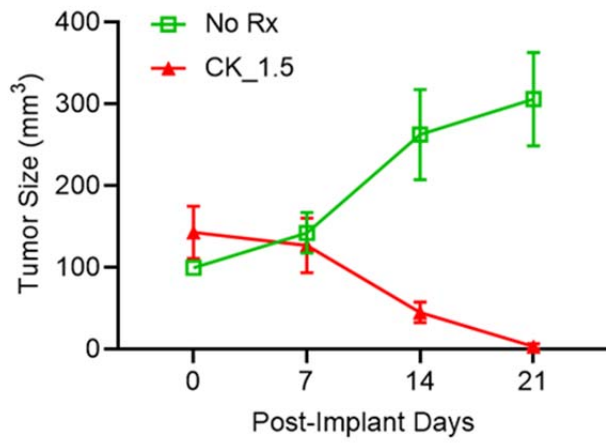
884

885

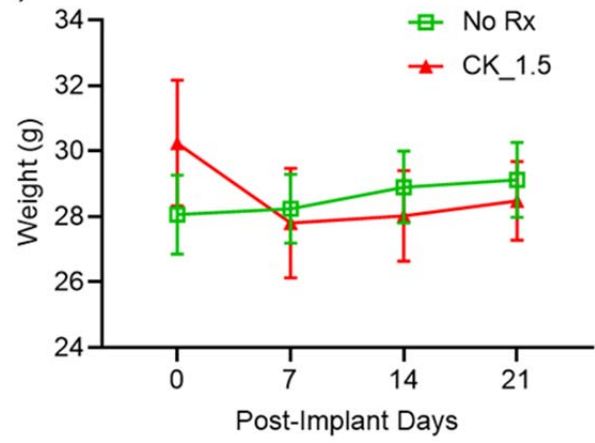
886

Figure 2-figure supplement 3. CK21 inhibited growth of Panc-1 tumors in a subcutaneous xenograft model. (a) Tumor growth with CK21 treatment at 3 mg/kg daily for 28 days. (b) Weight change of mice during Ck21 treatment.

(a)



(b)



887

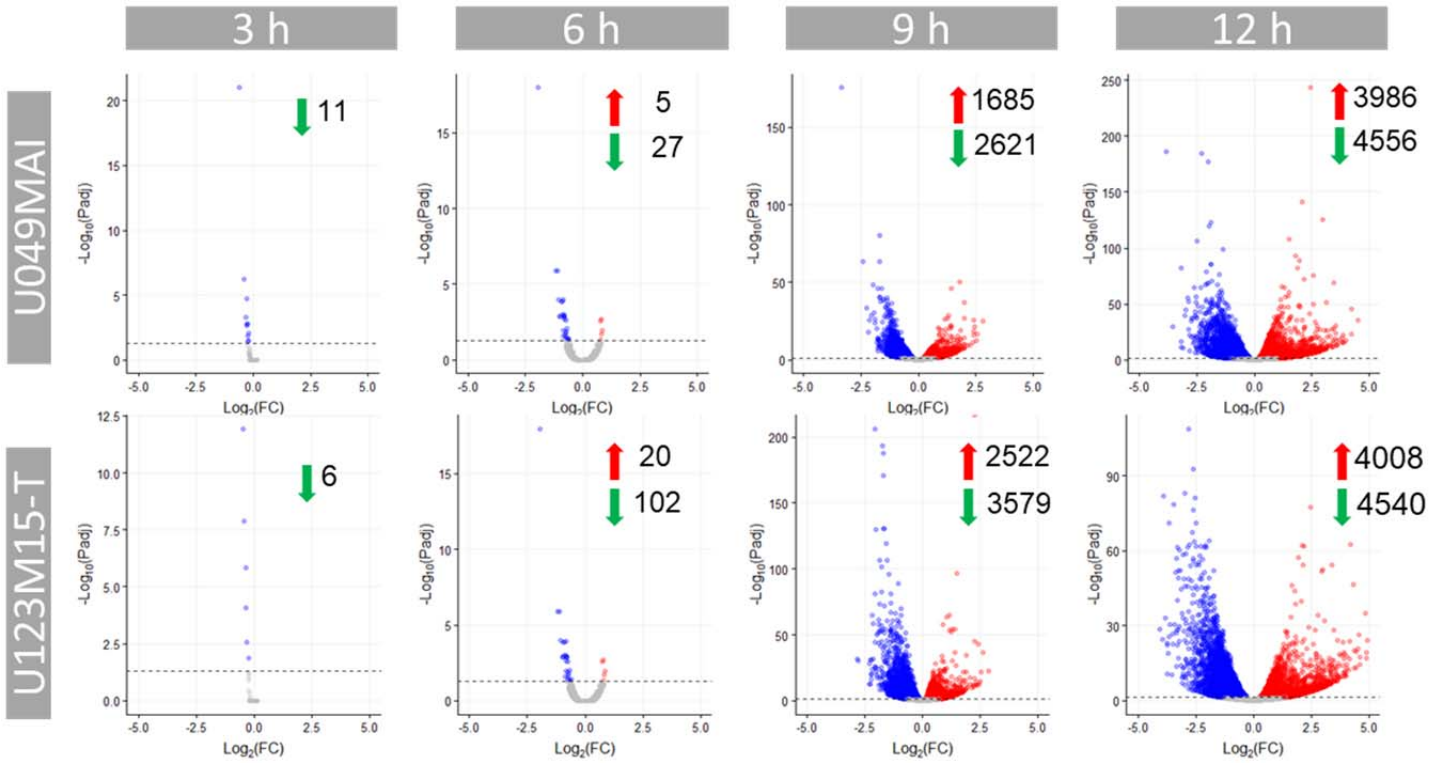
888

889

890

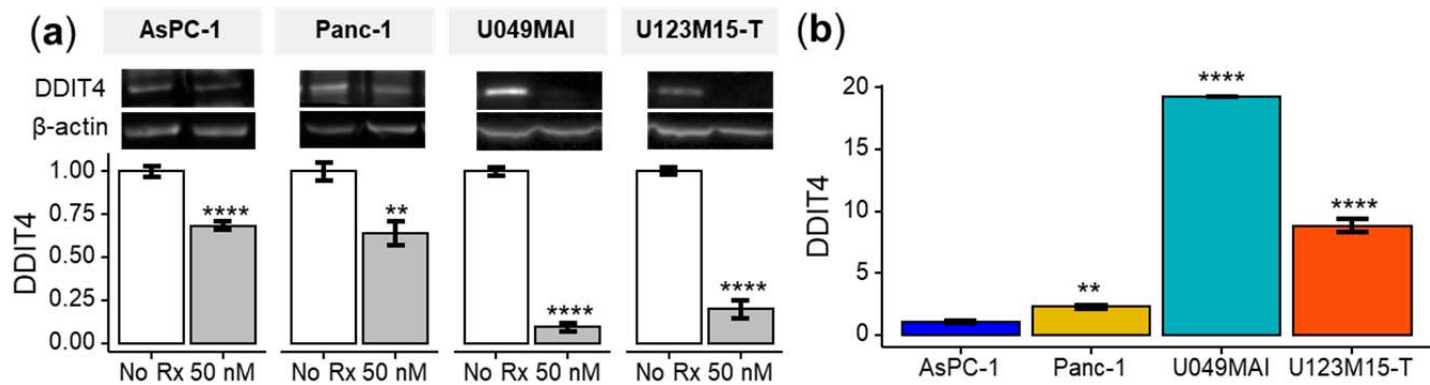
891

Figure 2-figure supplement 4. Male mice with AsPC-1 tumors responded to CK21. (a) Subcutaneous AsPC-1 tumor in male mice after CK21 treatment at 1.5 mg/kg. (b) Male mice weight during CK21 treatment. (N=5 for each experimental group)

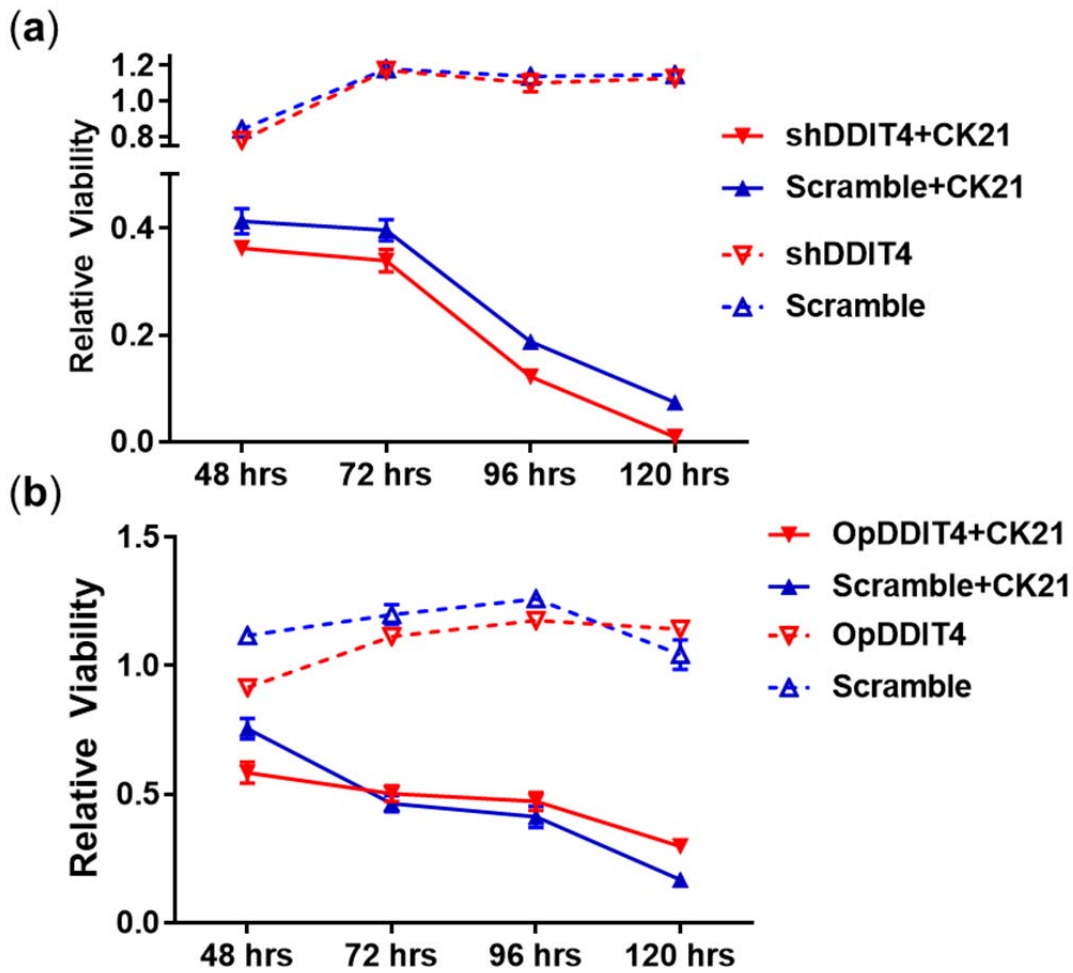


892
893
894
895

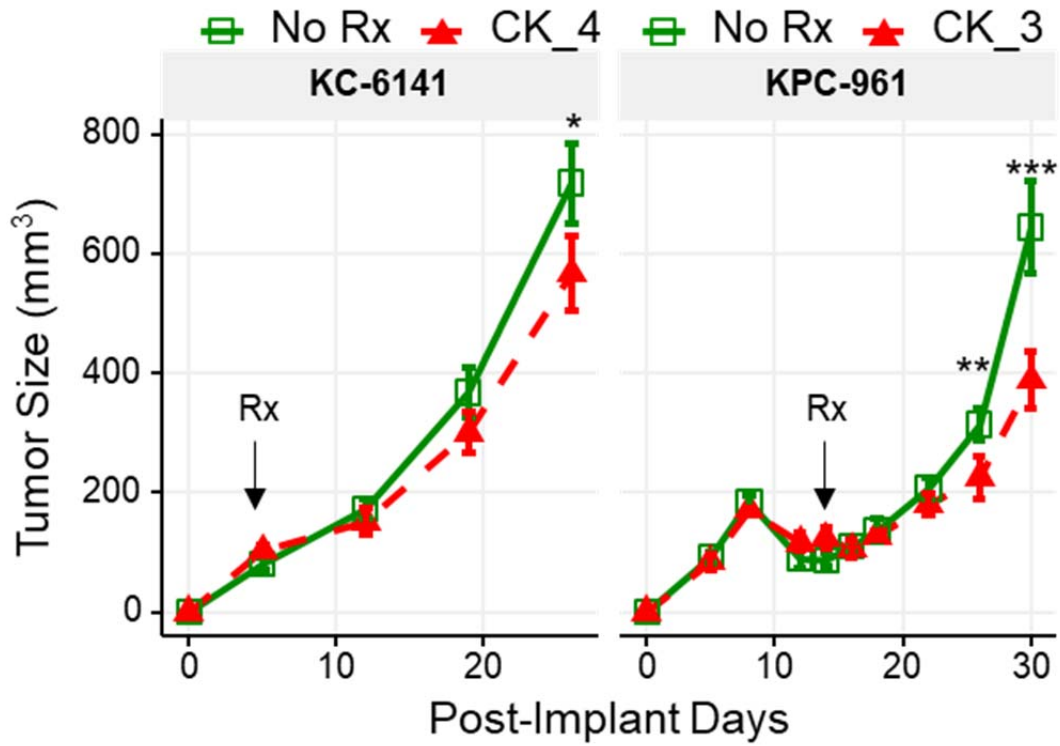
Figure 4-figure supplement 1. Volcano plots highlighting differentially expressed genes by U049MAI and U123m15-T respectively after 3h, 6h, 9h and 12 h of CK21 (50 nM) treatment.



896
897
898 Figure 4-figure supplement 2. (a) CK21 (50 mM) reduced the expression of DDIT4 in AsPC-1, Panc-1,
899 U049MAI, and U123M15-T after 24 hours of culture. (b) Baseline expression of DDIT4 in different tumor cells
900 (without CK21 treatment).
901

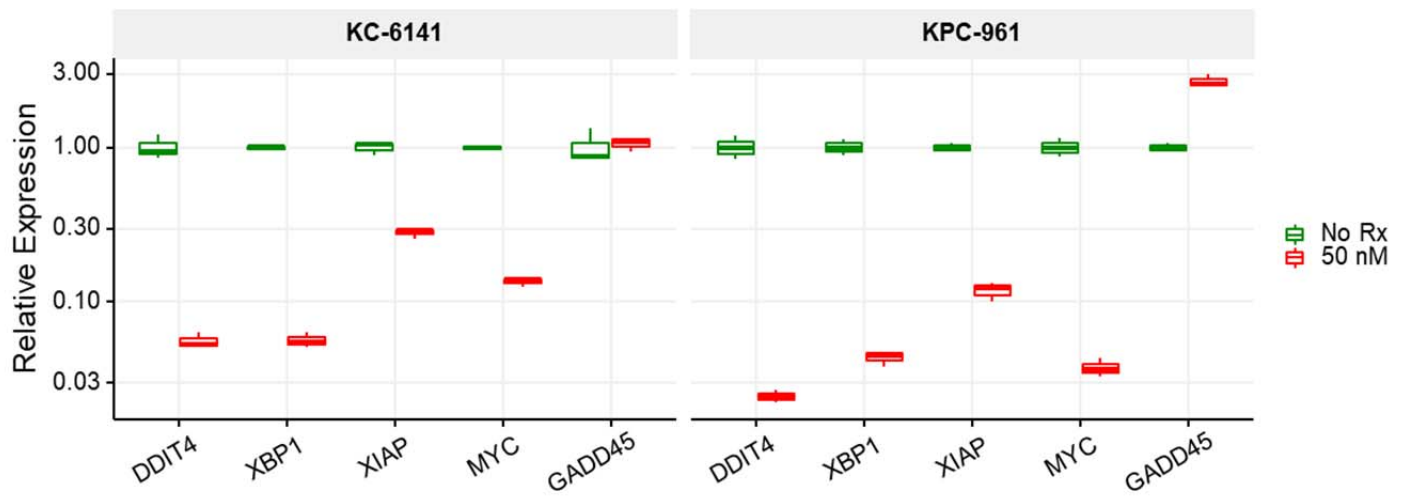


902 Figure 4-figure supplement 3. (a) knockdown of DDIT4 in Panc-1 did not alter response to CK21 (50 nM). (b)
 903 AsPC-1 overexpression of DDIT4 did not alter response to CK21 (50 nM).
 904
 905



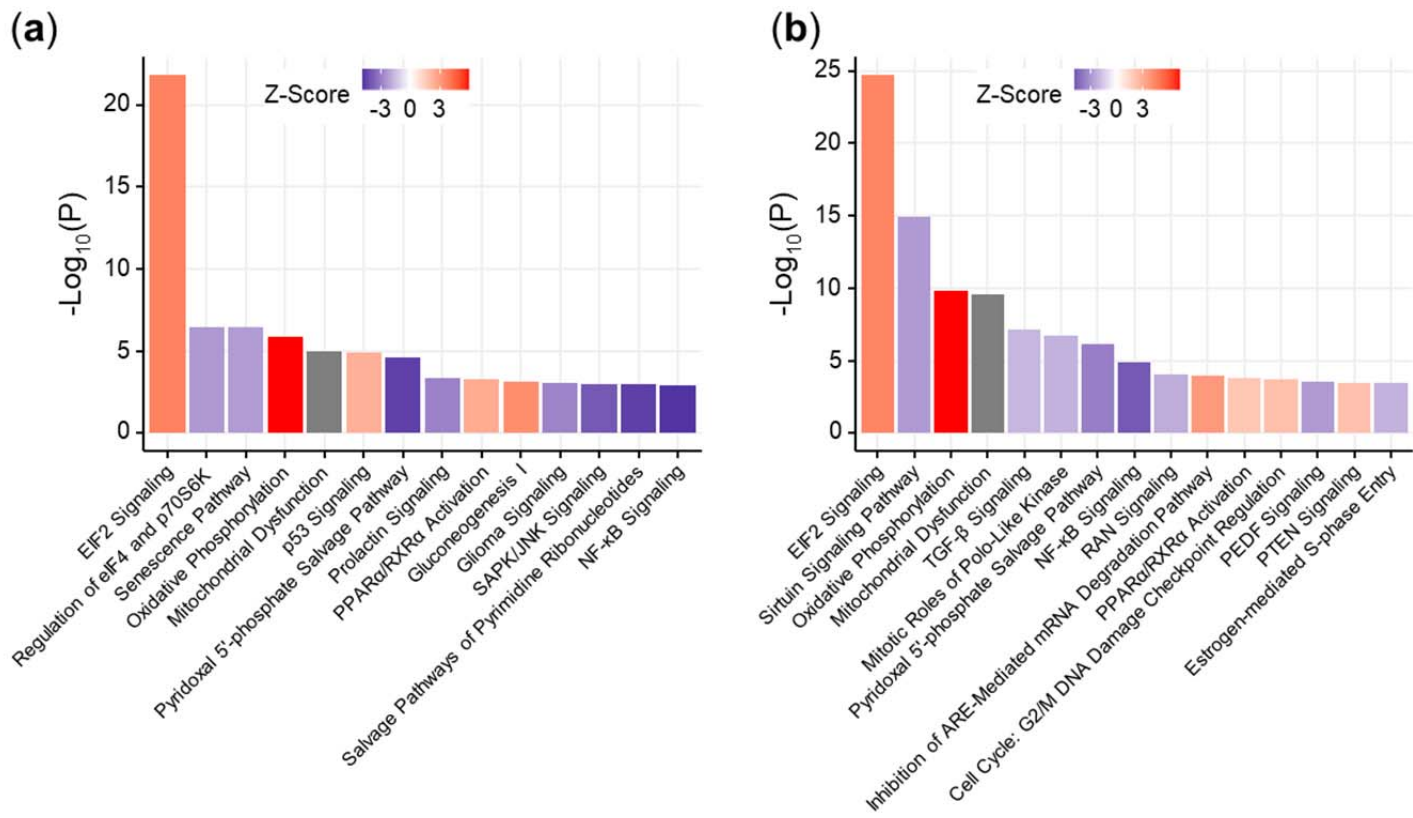
906
907
908
909
910

Figure 4-figure supplement 4. Tumor size of KC-6141 and KPC-961 after subcutaneous implantation in B6 or B6X129. CK21 given at 4 mg/kg/day for KC-6141 and 3 mg/kg/day for KPC-961 resulted in modest inhibition of tumor growth.



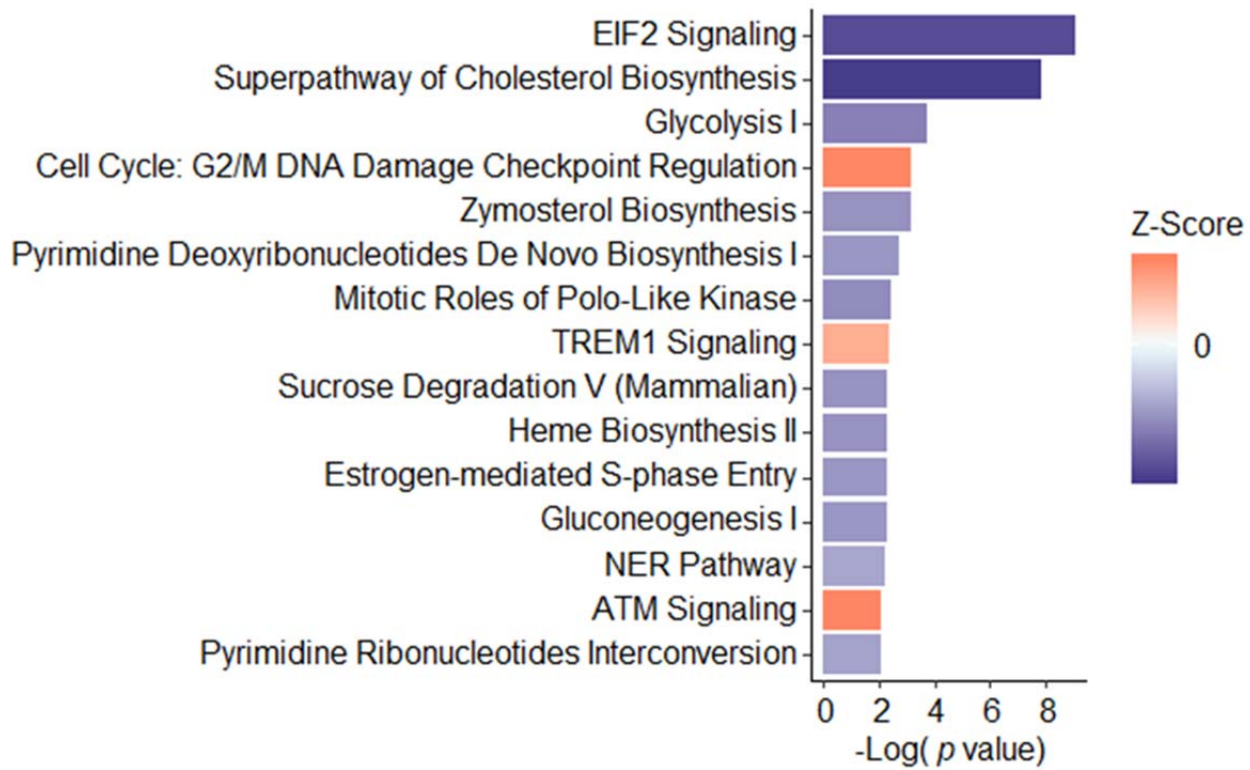
911
912
913
914

Figure 4-figure supplement 5. RT-qPCR analysis of differentially expressed genes by two mice pancreatic tumor cell lines after CK21 treatment at 50 nM for 24h.



915
916
917
918
919

Figure 5-figure supplement 1. Pathway enrichment of U049MAI and U123m15-T after treatment with CK21 (50 nM) for 9 hours. Top pathways for (a) U049MAI and (b) U123M15-T



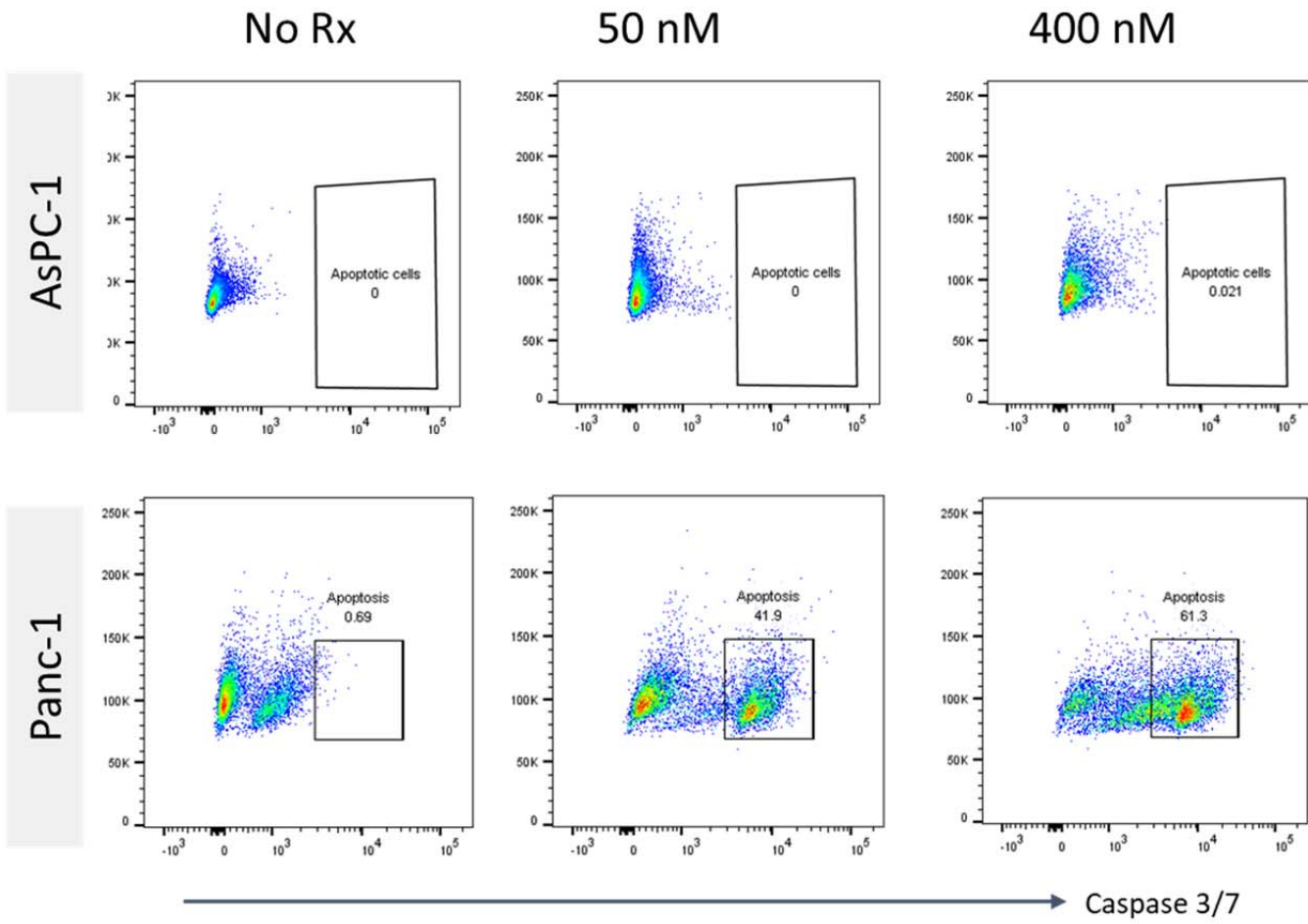
920

921

Figure 5-figure supplement 2. Pathway enrichment of orthotopic AsPC-1 tumors after treatment with CK21 (3 mg/kg) for 3 days.

922

923



924

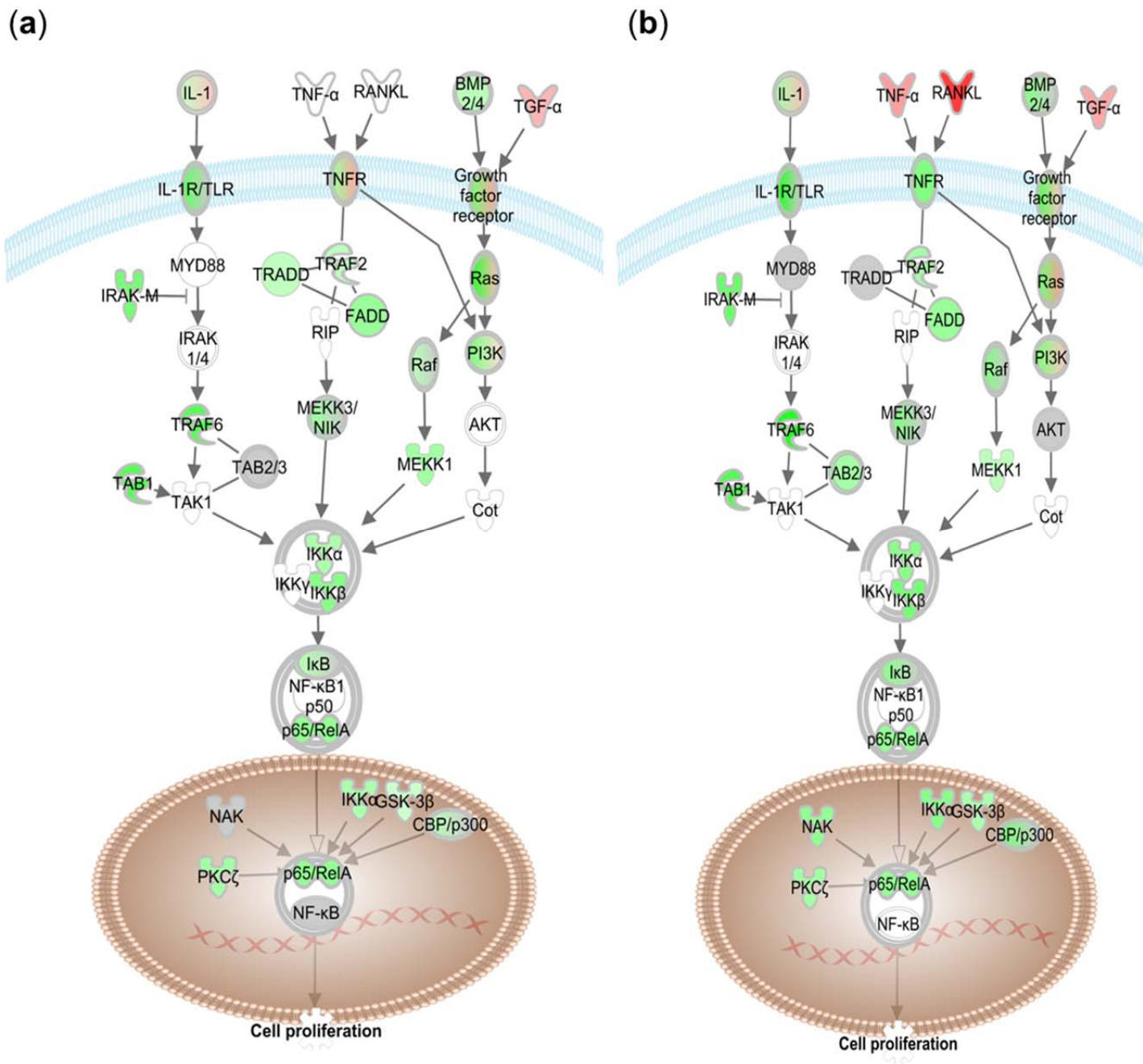
925

926

Figure 6-figure supplement 1. Flow plots illustrating active Caspase 3/7 expression in AsPC-1 and Panc-1 treated with CK21 (50 and 400 mM) for 24 hours.

927

928



929

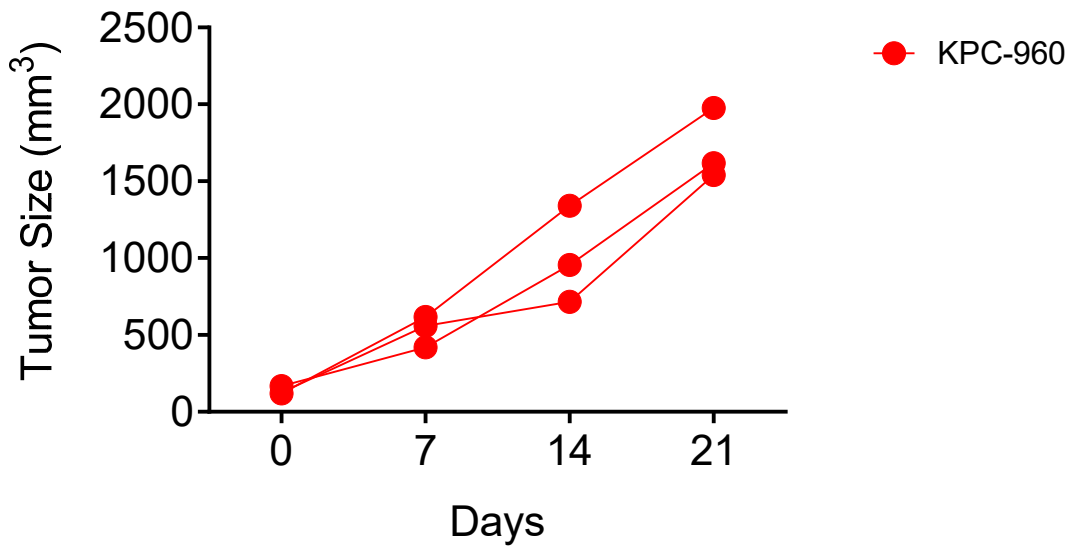
930

931

932

933

Figure 6-figure supplement 2. Key regulators in NF-κB canonical signaling pathway are significantly downregulated in (a) U049MAI and (b) U123m15-T after treatment with CK21 (50 nM) for 12 hours. Green represents downregulation and red represent upregulation by IPA analysis.



934
935
936
937

Figure 7-figure supplement 1. Tumor size of KPC-960 after subcutaneous implantation in nude mice. CK21 given at 3 mg/kg/day resulted in limited efficacy on tumor growth. Each line represents an animal.

938 **Figure source data**

939 Figure 1-source data1. Safety profile of CK21. Acute maximum tolerated dose (MTD) studies, toxicity and
940 toxicokinetic studies on rats and beagle dogs.

941
942 Figure 1-source data2. IC50 (μM) of triptolide (TP) or CK21 for different cancer cell lines in an in vitro cell
943 viability assay.

944
945 Figure 4-source data1. Essential information on the pancreatic tumor organoids used in this study. Details of
946 organoids from Patient# 1, 2, 6 and 7 are provided in reference 39 (Romero-Calvo et al., Molecular Cancer
947 Research 2019)

948
949 Figure 6-source data1. Full unedited gels.

i